

# Accepted Manuscript

A data-based landslide susceptibility map of Africa

Jente Broeckx, Matthias Vanmaercke, Rica Duchateau, Jean Poesen



PII: S0012-8252(17)30549-4  
DOI: [doi:10.1016/j.earscirev.2018.05.002](https://doi.org/10.1016/j.earscirev.2018.05.002)  
Reference: EARTH 2623  
To appear in: *Earth-Science Reviews*  
Received date: 25 October 2017  
Revised date: 26 April 2018  
Accepted date: 2 May 2018

Please cite this article as: Jente Broeckx, Matthias Vanmaercke, Rica Duchateau, Jean Poesen , A data-based landslide susceptibility map of Africa. *Earth-Science Reviews*(2017), doi:[10.1016/j.earscirev.2018.05.002](https://doi.org/10.1016/j.earscirev.2018.05.002)

This is a PDF file of an unedited manuscript that has been accepted for publication. As a service to our customers we are providing this early version of the manuscript. The manuscript will undergo copyediting, typesetting, and review of the resulting proof before it is published in its final form. Please note that during the production process errors may be discovered which could affect the content, and all legal disclaimers that apply to the journal pertain.

**A data-based landslide susceptibility map of Africa**

Jente Broeckx<sup>a,\*</sup>, Matthias Vanmaercke<sup>a,b,c</sup>, Rica Duchateau<sup>a</sup>, Jean Poesen<sup>a</sup>

<sup>a</sup>Department of Earth and Environmental Sciences, KU Leuven, Celestijnenlaan 200E, 3001 Heverlee, Belgium

<sup>b</sup>Université de Liège, Département de Géographie, Clos Mercator 3, 4000 Liège, Belgium

<sup>c</sup>Research Foundation Flanders (FWO), Egmontstraat 5, 1000 Brussels, Belgium

\*Corresponding author: Tel.: +3216379219, E-mail address:

Jente.Broeckx@ees.kuleuven.be

ACCEPTED MANUSCRIPT

**ABSTRACT**

Our understanding of the spatial patterns of landslides in Africa is limited with available landslide studies typically focusing on only one or a few study areas. Moreover, Africa is clearly underrepresented in terms of available landslide inventories. This study aims to produce a first continent-wide landslide susceptibility map for Africa, calibrated with a well-distributed landslide dataset. We reviewed the literature on landslides in Africa and compiled all available landslide inventories (ca. 10,800 landslides), supplemented by additional landslide mapping using Google Earth imagery in underrepresented regions (ca. 7,250 landslides). This resulted in a dataset of approximately 18,050 landslides. Various environmental variables were investigated for their significance in explaining the observed spatial patterns of landslides. To account for potential mapping biases in the dataset, we used Monte Carlo simulations that selected different subsets of mapped landslides to test the significance of the considered environmental variables. Based on these analyses, we constructed two landslide susceptibility maps for Africa: one for all landslide types and one excluding the known rockfalls. In both maps, topography is by far the most significant variable. We evaluated the performance of the fitted multiple logistic regression models using independent subsets of landslides, selected from the total dataset. Overall, both maps perform very well in predicting intra-continental patterns of landslides in Africa and explain about 80% of the observed variance in landslide occurrence. To further test the robustness and sensitivity to mapping biases, we also modelled landslide susceptibility while excluding regions with arid climates, as landslides in these environments are expected to be better preserved over time and therefore likely relatively overrepresented. Despite this potential bias, the effect on the landslide susceptibility model is limited. Based on the constructed database and our analyses we further discuss potential research gaps for landslide prediction in Africa and at continental scales. For example, analysis of the African countries' mean landslide susceptibility shows a lack of landslide research in various countries prone

to landsliding (e.g., Guinea, Gabon, Lesotho, Madagascar). Apart from the intrinsic value of this landslide susceptibility map as a natural hazard risk management tool, the map and compiled database are highly promising for other applications. For example, we explored the potential significance of landslides as a geomorphic process by confronting our landslide susceptibility map with an available database of measured catchment sediment yield for 500 rivers in Africa. Overall, a significant positive, but relatively weak relation between landslide susceptibility and sediment yield is observed.

## KEYWORDS

mass movement; landslide inventory; Google Earth; topography; seismicity; climate; air temperature; sediment yield

## ABBREVIATIONS

AUC: area under the ROC curve

LSD1: landslide dataset based on digitized landslide inventories

LSD2: landslide dataset based on mapped landslides in Google Earth

LSS: landslide susceptibility

MLR: mean local relief

P: mean annual precipitation

PGA: peak ground acceleration

ROC: receiver operating characteristic

SMA: maximum slope

std: standard deviation

SY: sediment yield

## 1. Introduction

Studies on landslide risks and fatalities indicate that landslides are present on all continents and are a global threat to humans, infrastructure and the environment (Dilley, 2005; Guzzetti et al., 2012; Haque et al., 2016; Kjekstad & Highland, 2009; Petley, 2012; Sassa & Canuti, 2009; Stanley & Kirschbaum, 2017). While this is certainly also the case for Africa, this continent remains strongly underrepresented in landslide research (e.g. Gariano & Guzzetti, 2016; Kirschbaum et al., 2015, 2010; Maes et al., 2017; Nadim et al., 2006; Petley, 2012; Reichenbach et al., 2018). Also global landslide susceptibility (*LSS*) maps rely on very few (or no) data of observed landslides in Africa for their calibration (e.g. Hong et al., 2007; Kirschbaum et al., 2009; Nadim et al. 2006; Stanley & Kirschbaum, 2017). Nonetheless, landslides are one of the deadliest natural disasters in Africa (Guha-Sapir et al., 2017). Moreover, their importance and impact are expected to increase due to climate change, with an increase in total precipitation and increasing frequency and intensity of rainstorm events (Gariano & Guzzetti, 2016). This was for instance shown for the Great Lakes region (Shongwe et al., 2011; Souverijns et al., 2016; Thiery et al., 2016), probably one of the most landslide susceptible regions in Africa (Hong et al., 2007; Stanley & Kirschbaum 2017). In addition, Africa is facing a considerable growth in population, which is projected to triple by the end of the 21<sup>st</sup> century (Gerland et al., 2014). This will likely affect both the frequency and impact of landslide events. For these reasons, earlier studies have urged to fill the gap on landslide research in Africa (e.g. Gariano & Guzzetti, 2016; Jacobs et al., 2016; Maes et al., 2017).

Furthermore, our geomorphic understanding of erosion processes at a continental scale may significantly benefit from addressing this research gap. Several studies indicate the importance of landslides as a dominant process explaining variations in catchment sediment yield (*SY*, [ $\text{t km}^{-2} \text{y}^{-1}$ ]) at regional and continental scales (e.g. Broeckx et al., 2016; Delmas et al., 2009; de Vente et al., 2006; Vanmaercke et al.,

2017). As with landslides, information on *SY* for Africa is relatively scarce. However, Vanmaercke et al. (2014) demonstrated highly significant correlations between spatial patterns of contemporary *SY* and spatial patterns of seismicity in Africa. This indicates that landsliding could also play a significant role in the sediment budget of Africa, given that seismic activity can trigger landslides, but may also increase the susceptibility to landsliding by weakening substrates (e.g. Broeckx et al., 2016; Chang et al., 2007; Chuang et al., 2009; Hovius et al., 2011; Marc et al., 2015; Molnar et al., 2007; Nowicki et al., 2014; Vanmaercke et al., 2017). On the whole, the importance of landslides for *SY* in different environments remains poorly understood and our ability to simulate this process at larger spatial scales remains limited (Broeckx et al., 2016; de Vente et al., 2013; Hovius et al., 2011; Korup et al., 2014). Nevertheless, recent research showed the promising potential of *LSS* maps as a tool to better assess the importance of landsliding for catchment *SY* at such scales (Broeckx et al., 2016).

Overall, this paper aims to contribute to a better understanding of landslide susceptibility in Africa and its importance as a geomorphic process. More specifically, we (1) carried out a review on mapped landslides in Africa and present an extensive compilation of this data; (2) propose a first continent-wide *LSS* map of Africa, calibrated by well-distributed landslide data; (3) explore the relation between *LSS* and *SY* for Africa; and (4) indicate scopes for further landslide research in Africa and at continental scales, based on a critical discussion of the compiled database and its analyses.

## **2. Materials and methods**

### **2.1. Landslide data collection**

#### **2.1.1. Available landslide inventories**

The first step towards an African LSS map, encompassed the compilation of available landslide inventories for Africa. This was done through an extensive literature review of scientific papers, PhD and MSc theses and research institution websites (e.g.: Royal Museum for Central Africa, 2016). All landslide inventories suitable for digitization and georeferencing were selected from this review. Inventories required precise landslide coordinates (e.g. Mansour et al., 2014), the presence of a coordinate grid (e.g. Ayonghe et al., 2004) or other landscape features that allowed a sufficiently accurate georeferencing of the landslide inventory map (e.g. Moeyersons et al., 2004). A second selection retained those inventories with estimated errors on landslide locations of less than 12'' (corresponding to ca. 350 m across the African continent). This error was estimated based on the quality and level of detail of the landslide features on the map and the average georeferencing error. The latter was assessed by exporting the digitized and georeferenced inventory maps to Google Earth and measuring the distance between clear landscape features (e.g. roads) on the map and on Google Earth images for a number of control points (typically 5). This resulted in a first landslide dataset (*LSD1*) based on digitized landslide inventories from the literature.

### **2.1.2. Additional landslide mapping in Google Earth**

Our literature review indicated that most studies focused on only a limited number of African countries and areas. Moreover, studies indicate that in many landslide-prone countries, little or no landslide research has been conducted (e.g. Gariano & Guzzetti, 2016; Jacobs et al., 2016, 2017; Maes et al., 2017). To improve the completeness and spatial representativeness of our landslide dataset, we generated a second landslide dataset (*LSD2*) by mapping additional landslides that could be observed in Google Earth imagery. Mapped landslides in this dataset include landslides in the study areas of the digitized inventories (2.1.1) that were not included in the inventory (e.g. missed or more recent landslides), as well as landslides in other

regions. Efforts to map additional landslides in other regions concentrated on areas that were known to be susceptible, e.g. based on studies that could not be accurately geo-referenced, local studies that provided no inventory, but reported the presence of landslides and earlier developed (global) landslide susceptibility maps (e.g. Audru et al., 2010; Nadim et al., 2006). However, also other areas were investigated for the presence of landslides. We did not intend to create a complete dataset of landslides in the mapped areas, but one with a good spatial coverage to represent the entire African continent. Examples of landslides mapped with Google Earth are shown in Fig. 1. Each landslide in Google Earth was mapped as a point, located at the landslide scarp. Landslide typology was not assessed in detail, apart from rockfalls that were considered as a separate category.



**Fig. 1. Examples of landslides mapped in Google Earth. Tanzania (10.929°S, 39.547°E), Angola (15.194°S, 13.210°E), Lesotho (29.145°S, 28.024°E, rockfall), Comoros (12.230°S, 44.420°E).**

### 2.1.3. Mapping of non-landslide points

If landslide inventories are correct and complete, they also indicate the locations in the study area where landslides are absent (Guzzetti et al., 2012). However, we found that most of the landslide inventories were incomplete. This was sometimes

reported by the landslide studies themselves or because these studies considered only landslides linked to a specific event (e.g. earthquake) and hence presented no geomorphological historical inventory (e.g. Agbor et al., 2014; Bouhadad et al., 2010). Besides, the incompleteness of inventories was also observed by comparing digitized landslide numbers with reported landslide numbers and by examining the study areas in Google Earth. Also the landslides we mapped based on Google Earth remain incomplete (2.1.2). Given our intent to assess *LSS* at the continental scale, the completeness of the landslide inventories was not considered as a quality criterion. Nevertheless, both landslide and non-landslide observations are required to correctly calibrate a logistic *LSS* model. To limit potential errors of including false negatives (i.e. non-landslide points that in fact correspond to landslide areas), we also generated a dataset of non-landslide locations. 2050 points were randomly distributed across Africa, at least one kilometer away from the known landslides. Each point was visually checked in Google Earth for the presence or absence of landslides. This approach had several advantages: (1) the entire African continent is correctly represented and not just the most susceptible areas covered by landslide studies; (2) all non-landslide points have exact locations; (3) chances of randomly selecting landslide locations are small as most locations are free of landslides and generating random points outside the most susceptible areas further reduces the chance of false negatives; (4) a visual check in Google Earth allowed for an additional removal of false negatives (<5%). Hence, although not all landslides can be seen in Google Earth, this method allowed for a representative and well distributed dataset of locations that are unlikely to be affected by landslides.

## **2.2. Environmental variables**

Based on a review on landslide conditioning factors (Pourghasemi & Rossi, 2017), five independent environmental factors with available data for Africa were considered (i.e. topography, lithology, land use, precipitation and seismicity). For the logistic

regression analyses, six quantitative and seven qualitative variables that describe these factors were derived (Table 1). The qualitative variables, represent the most common lithological classes in Africa (Hartmann & Moosdorf, 2012) and were transformed into seven dummy variables, each having a value of 1 or 0, indicating the presence or absence of that particular lithology, respectively. The selected parameters correspond to variables typically selected in similar LSS studies (e.g. Budimir et al., 2015; Stanley & Kirschbaum, 2017; Van Den Eeckhaut et al., 2012) and are based on GIS data, with a consistent coverage for the entire African continent. All variables were rescaled to a resolution of 12", i.e. larger than the maximum estimated positional error on the mapped landslides (2.1.1) and equal to the resolution of the resulting LSS maps. This rescaling implied a decrease in resolution with a factor four for the topographic data (3" SRTM). For this, both the maximum slope (SMA) and the mean local relief (MLR) were calculated in a 4x4 grid. The resulting values were then aggregated to a new raster at a resolution of 12".

**Table 1. Overview of the considered variables. 'na' indicates not applicable. All variables were rescaled to a resolution of 12" for the analyses.**

Variable	Description	Unit	Resolution	Source
SMA	maximum slope within a 4x4 SRTM 3" slope grid.	%	3"	USGS
MLR	mean local relief within a 4x4 SRTM 3" slope grid. Where local relief is the maximum altitude difference within a circle with a radius of 5 km at the equator	m	3"	USGS
PGA	peak ground acceleration with an exceedance probability of 10% in 50 years	m s <sup>-2</sup>	0.1"	Giardini et al., 1999; Shedlock et al., 2000
P	precipitation: average (1961-1990) annual rainfall	mm	0.16°	New et al., 2002
RDN	rainy day normal: total annual rainfall divided by the number of rainy days	mm/day	0.16°	New et al., 2002
TREE	tree cover: fraction of a pixel covered by trees (1992-1993 satellite data)	%	30"	DeFries et al., 2000
SU	unconsolidated sediments: lithological class applied as a dummy variable	na	2 km	Hartmann & Moosdorf, 2012
SS	siliciclastic sedimentary rocks: lithological class applied as a dummy variable	na	2 km	Hartmann & Moosdorf, 2012
SM	mixed sedimentary rocks: lithological class applied as a dummy variable	na	2 km	Hartmann & Moosdorf, 2012
SC	carbonate sedimentary rocks: lithological class applied as a dummy variable	na	2 km	Hartmann & Moosdorf, 2012
PL	plutonic rocks: lithological class applied as a dummy variable	na	2 km	Hartmann & Moosdorf, 2012
MT	metamorphics: lithological class applied as a dummy variable	na	2 km	Hartmann & Moosdorf, 2012
VOLC	volcanic rocks: lithological class applied as a dummy variable	na	2 km	Hartmann & Moosdorf, 2012

### 2.3. Logistic landslide susceptibility model

Logistic regression is a widely used technique in landslide susceptibility modelling (e.g. Ayalew & Yamagishi, 2005; Budimir et al., 2015; Dai & Lee et al., 2002; Vanacker et al., 2003; Van Den Eeckhaut et al., 2012, 2010, 2006). It describes the

relationship between a set of independent variables and a binary dependent variable, i.e. the presence or absence of a landslide. The logistic function can be written as (Kleinbaum & Klein, 2010):

$$p(\mathbf{y} = \mathbf{1}) = \frac{1}{1 + e^{-(b_0 + b_1x_1 + b_2x_2 + \dots + b_nx_n)}} \quad \text{equation 1}$$

With  $p$  the probability of landslide occurrence,  $x_i$  the dependent variables and  $b_i$  the regression coefficients. The result of this equation is a number between 0 and 1, which can be interpreted as the probability that a landslide occurs under the given set of variable values (Kleinbaum & Klein, 2010). When fitting logistic regression models with only one parameter, the Wald test statistic is commonly used to test the significance of the coefficients  $b_i$ , which is obtained by comparing the maximum likelihood estimate of  $b_i$  with its standard error (Kleinbaum & Klein, 2010).

We considered the Wald test statistic at the 0.01 significance level, to determine the significance of individual environmental variables in predicting *LSS*. For each considered variable separately, we first fitted five univariate logistic regression models by randomly selecting respectively 500, 1000, 2000, 4000 and 8000 points from the entire dataset of landslide and non-landslide locations. In a next step, different combinations of all significant independent variables were tested in a multiple logistic regression approach. We performed two parallel analyses: one for all landslide types (*LS (all)*) and one excluding the rockfalls that were mapped in Google Earth (*LS (excl. rockfalls)*). Mc Fadden's pseudo  $R^2$  ( $R_{\text{McF}}^2$ ) was used as a measure of goodness-of-fit, similar to the coefficient of determination for linear models (Cameron & Windmeijer, 1997). P-values were used to test the statistical significance ( $p < 0.01$ ) of the predictor variables in the model.

As discussed above (section 2.1), landslide inventories were derived from various sources and consequently reflect large differences in the number and density of landslides. As a result, some combinations of environmental variables (Table 1) may be overrepresented in the landslide dataset. To account for these potential biases in our models, we first aggregated the digitized landslides at the pixel level (resolution of 12''), i.e. for all pixels containing more than one landslide point, only one of them was retained after random selection. We further reduced the number and density of landslides in the inventories according to three selection rules: (1) all landslides are retained for inventories with less than 50 landslides. (2) for inventories with more than 50, 100 and 200 landslides, the number of landslides was iteratively reduced to obtain a density smaller than respectively 2, 0.5 and 0.1 landslides/km<sup>2</sup>, with a lower limit of respectively 50, 100 and 200 landslides. (3) maximum 300 landslides were retained from any individual inventory. The correct number of landslides was randomly selected from each inventory, as a heuristic way to give a balanced weight to all landslide inventories. Landslides mapped in Google Earth in a specific area or clearly representing one triggering event, were also considered as an inventory to which these selection rules were applied.

From this generated subset, 2/3 of the landslides were then randomly selected for model calibration and 1/3 for model validation. This procedure was repeated 101 times for each combination of significant independent variables, since it was assessed that the range of  $R_{McF}^2$  values did not significantly increase for larger numbers of iterations. Overall, this Monte Carlo simulation approach allowed us to select the most appropriate *LSS* models (for all landslides and after excluding known rockfalls). Furthermore, it allowed for the mapping of the standard deviation of obtained *LSS* values for each pixel and, hence, to identify areas with larger and smaller uncertainties in estimated *LSS* across Africa.

To evaluate model performance, receiver operation characteristic (ROC) curves were produced and analysed. ROC curves are a widely used technique in LSS model validation and useful for selecting LSS class boundaries for the final LSS maps. Class boundaries were chosen, based on natural breaks with the aim to include as many landslides as possible in the highest susceptibility classes covering areas as small as possible (e.g. Balteanu et al., 2010; Pontius & Schneider, 2001; Pradhan, 2013; Swets, 1988; Van Den Eeckhaut et al., 2012). ROC curves are considered a more appropriate validation technique than success and prediction rate curves, since they are independent of the relative frequencies of landslide versus non-landslide pixels (Swets, 1988; Van Den Eeckhaut et al., 2009b). ROC curves were constructed for the total landslide subset and for six randomly selected validation datasets, used in the Monte Carlo simulations.

#### **2.4. Landslide susceptibility modelling, excluding arid climates**

In many cases, older landslides are difficult to detect as their scars are covered by vegetation and remodelled by other geomorphic processes (e.g. creep, erosion, sediment deposition). The rate at which this happens likely depends on the climate, with older landslides being more likely to be preserved in more arid climates. This may lead to biases in continental-scale LSS models as presented here. To assess the importance of these potential biases, we constructed an additional landslide map by applying the Köppen-Geiger climate classification and excluded all landslides in regions of B-type (arid) climates (Peel et al., 2007) from the landslide inventory. With this subset, we then performed logistic regression analyses as described in section 2.3.

#### **2.5. Relation between landslide susceptibility and catchment sediment yield**

Vanmaercke et al. (2014) compiled a large dataset of measured SY data for Africa. These data were either collected from gauging station measurements or derived from

a reservoir sedimentation rate, with median measuring periods of 4 and 17 years respectively. The catchment areas range between 0.02 and  $3.8 \times 10^6$  km<sup>2</sup> (median 998 km<sup>2</sup>). We investigated the explanatory power of *LSS* for *SY*, by calculating the average catchment *LSS* and exploring correlations with measured *SY* for 500 catchments for which the catchment boundaries could be correctly delineated. Only catchments for which the delineated catchment area deviated less than 20% from the reported area were retained. However, the median deviation between reported and delineated area was less than 3%. We considered the *LSS* model excluding rockfalls, as this landslide type is not expected to directly contribute to suspended sediment yield in rivers. Spearman correlation was considered as a goodness of fit measure, since neither *SY*, nor mean *LSS* were normally distributed.

### 3. Results and discussion

#### 3.1. Landslide datasets

An overview of all compiled landslide data is presented in Fig. 2. Combined, the dataset based on available inventories (*LSD1*) and the dataset of additional landslides mapped in Google Earth (*LSD2*) contain 18053 landslides, covering 51 out of 55 African countries and the island of Reunion. *LSD1* is the largest dataset. By reviewing the literature, we found over 200 potentially relevant publications with landslide data for Africa. From these publications, 60 landslide inventories could be digitized (Table 2). Of these, 49 inventories were of sufficient quality (section 2.1.1) and were retained in *LSD1* (10817 landslides). Additional mapping in Google Earth, guided by studies from our literature review and focusing on data-scarce regions resulted in a second dataset of 7236 landslides (*LSD2*).

Several global landslide inventories exist that also cover Africa to some extent (e.g. Kirschbaum et al., 2010; Petley, 2012). Mapped landslides in these databases, were not directly used in this study due to the spatial uncertainty of landslide locations

(section 2.1.1). However, a visual comparison shows that our landslide dataset covers all regions of Africa that are represented in these global studies. Overall, both the number and the spatial coverage of landslides in our dataset is much larger and more representative for the African continent. This difference is partly due to the focus of those studies on rainfall-induced landslides (Kirschbaum et al., 2010) or landslides causing fatalities only (Petley, 2012). Despite these differences in extent and focus of these two global studies, we find the same landslide hotspots in our study (Fig. 2). The same pattern of hotspots in terms of landslide studies can be found in Maes et al. (2017). They give a spatial overview of publications on landslides and on landslide risk reduction measures in the tropics.

More specifically, our dataset contains many landslides in the northernmost regions of Maghreb countries, e.g.: Morocco, Algeria and Tunisia, and West-Africa with numerous studies in Cameroon. However, most studies cover the East-African Rift region with Ethiopia, Uganda, DR Congo, Tanzania, Malawi and South-Africa contributing most of the landslides to our dataset. These landslide numbers can give a first indication of *LSS*, but are certainly not a true representation of the spatial distribution of landslide frequencies across Africa, since we did not intend to produce a complete dataset of landslides for Africa (section 2.1.2). For example, the dataset contains over 1000 landslides mapped in detail in Google Earth for a single region in Angola, corresponding to a heavy rainfall event (Dinis et al., 2013). On the other hand, many regions in South-Africa were mapped, where not all observed landslides were digitized. Moreover, the identification of landslides can be biased by the spatial and temporal resolution and availability of satellite imagery for different regions. In addition, one has to bear in mind that the observed landslide frequency is affected by differences in periods of landslide scar conservation across the African continent due to the diversity in climates (see discussion in section 3.2.3). Therefore, even a

complete inventorialisation of landslides across Africa would not be a correct representation of the landslide occurrence across the continent.

These spatial differences in landslide representation may potentially bias assessments of *LSS* and should be taken into account in *LSS* analyses (see sections 2.3 and 2.4). Likewise, the landslides included in our dataset typically have an unknown age and are not necessarily representative for actual contemporary landslide frequencies. As a result, this study only aims to seek and explain the spatial patterns in *LSS* in Africa. The rate or hazard of landslide events is beyond the scope of this study.

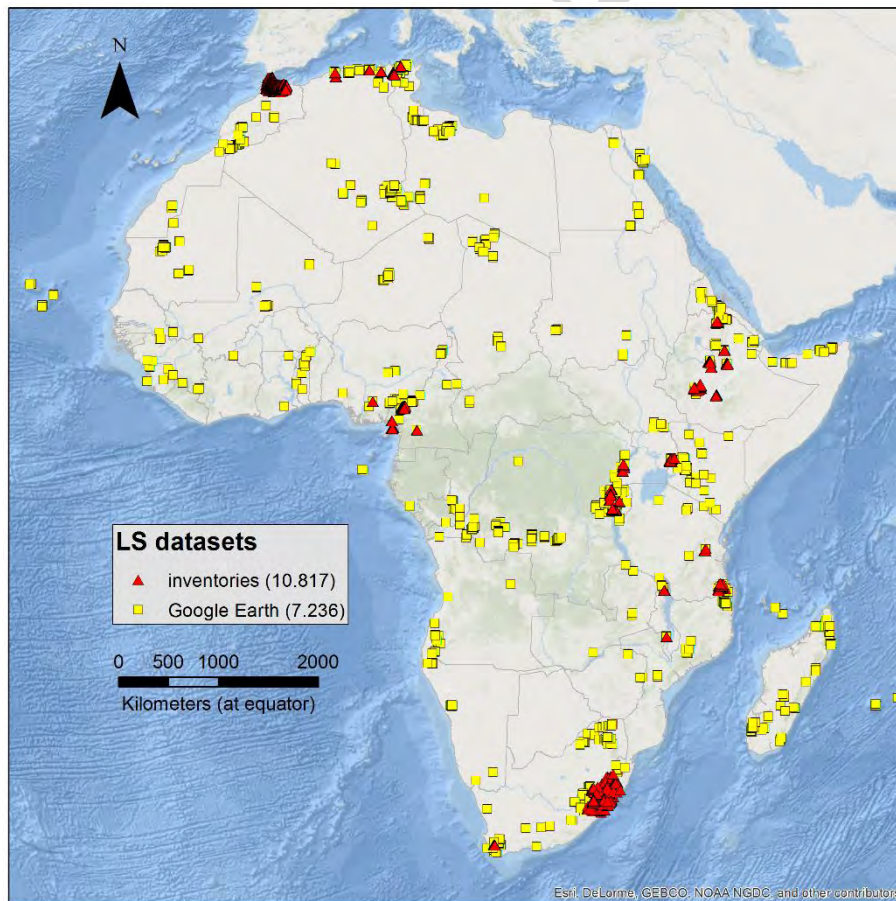


**Fig. 2. Spatial overview of all compiled landslide locations in Africa, classified by dataset LSD1: inventories, LSD2: Google Earth (section 2.1).**

**Table 2: Overview of all mapped landslides by country (LSD1: inventories, LSD2: Google Earth). References of landslide inventories used in our analyses (n=49) are marked in bold. Other listed references on landslides were used as a guide to map landslides in Google Earth.**

Country	# LS in LSD1 (# inventories)	# LS in LSD2	total # LS	sources
Algeria	266 (5)	322	588	Bouhadad, 2010; <b>Bourenane et al., 2015</b> ; Busche, 2001; <b>Capot-Rey, 1954</b> ; <b>Gabert, 1984</b> ; <b>Hadji et al., 2013</b> ; <b>Mansour et al., 2014</b> ; Raunet, 1973
Angola	0 (0)	1308	1308	Dimis et al., 2013
Benin	0 (0)	8	8	
Burkina Faso	0 (0)	3	3	
Burundi	87 (1)	117	204	<b>Nibigira et al., 2013</b>
Cabo Verde	0 (0)	93	93	
Cameroon	440 (6)	145	585	<b>Afungang, 2015</b> ; <b>Ayonghe et al., 2004, 1999</b> ; <b>Che et al., 2011</b> ; <b>Ngatcha et al., 2011</b> ; <b>Ngole et al., 2007</b> ; Zogning et al., 2007
Central African Republic	0 (0)	6	6	
Chad	0 (0)	87	87	
Comoros	0 (0)	33	33	Audru et al., 2010
Congo Republic	0 (0)	77	77	
Cote d'Ivoire	0 (0)	2	2	
Djibouti	0 (0)	33	33	
DR Congo	231 (4)	685	916	<b>Maki Mateso &amp; Dewitte, 2014</b> ; <b>Moeyersons et al., 2010, 2004</b> ; Ndyanabo et al., 2011; Royal Museum for Central Africa, 2016; Sahani, 2011
Egypt	0 (0)	120	120	Arnous, 2011; Emam et al., 2010
Eritrea	0 (0)	74	74	
Ethiopia	700 (9)	101	801	<b>Asfaw, 2010</b> ; <b>Asma, 2013</b> ; <b>Broothaerts et al., 2012</b> ; <b>Girma, 2010</b> ; <b>Hagos, 2012</b> ; <b>Ismail, 2013</b> ; <b>Suyum, 2011</b> ; <b>Temesgen et al., 2001</b> ; <b>Van Den Eeckhaut et al., 2009</b> ; <b>Vercammen, 2011</b>
Gabon	0 (0)	31	31	
Ghana	0 (0)	16	16	
Guinea	0 (0)	23	23	
Guinea-Bissau	0 (0)	0	0	
Kenya	0 (0)	325	325	Maina-Gichaba et al., 2013; Ngecu & Mathu, 1999
Lesotho	0 (0)	35	35	
Liberia	0 (0)	6	6	
Libya	0 (0)	174	174	Busche, 2001; Ostaficzuk, 1973
Madagascar	0 (0)	411	411	Ramasiarinoro et al., 2012
Malawi	130 (4)	47	177	<b>Msilimba, 2010</b> ; <b>Msilimba &amp; Holmes, 2010</b>
Mali	0 (0)	35	35	
Mauritania	0 (0)	129	129	Busche, 2001
Mauritius	0 (0)	5	5	
Morocco	3600 (1)	150	3750	Choubert & Ennadifi, 1970; <b>Fonseca, 2014</b>
Mozambique	0 (0)	334	334	Bomans, 2005
Namibia	0 (0)	50	50	
Niger	0 (0)	146	146	Busche, 2001
Nigeria	43 (1)	148	191	Agbor et al., 2014; <b>Igwe &amp; Fukuoka, 2014</b> ; Okagbue, 1994
Reunion	0 (0)	21	21	
Rwanda	30 (2)	42	72	<b>Moeyersons, 2003</b> ; <b>Moeyersons et al., 2004</b>
Sao Tome and Principe	0 (0)	5	5	
Senegal	0 (0)	2	2	
Sierra Leone	0 (0)	13	13	
Somalia	0 (0)	73	73	
South Africa	3349 (4)	1050	4399	<b>Bijker, 2001</b> ; Chiliza & Richardson, 2008; De Lemos, 2013; <b>Gupta, 2001</b> ; <b>Hardwick, 2012</b> ; <b>Singh, 2009</b> ; Tyoda et al., 2012
South Sudan	0 (0)	45	45	
Sudan	0 (0)	41	41	
Swaziland	0 (0)	10	10	
Tanzania	788 (3)	170	958	<b>Bomans, 2005</b> ; <b>Kimaro et al., 2010</b> ; <b>Temple &amp; Rapp, 1972</b>
Togo	0 (0)	11	11	
Tunisia	342 (1)	246	588	<b>Bonvallot, 1984</b> ; Busche, 2001; Dimanche & Hamza, 1978
Uganda	811 (8)	156	967	Broeckx et al., in prep.; <b>Jacobs et al., 2016, 2017</b> ; <b>Knapen et al., 2006</b> ; <b>Maertens, 2016</b>
Western Sahara	0 (0)	29	29	
Zambia	0 (0)	36	36	
Zimbabwe	0 (0)	7	7	
<b>Total</b>	<b>10817 (49)</b>	<b>7236</b>	<b>18053</b>	

### 3.2.1. Controlling factors and calibration of the landslide susceptibility maps

Processing of the data for the *LSS* analyses, as described in section 2.3, resulted in a dataset of 9652 points used for model calibration, corresponding to 7641 landslides and 2011 non-landslide locations. The ratio between non-landslide and landslide pixels is 0.26, which is within the suggested range of 0.2 to 1 by King and Zeng (2001). However, Allison (2012) states that small samples (<200 occurrences: absolute rareness) rather than extreme proportions (relative rareness) are problematic for valid logistic regression results. With 2011 non-landslide locations also this criterion is met. Tests (carried out before model calibration), in which the number of non-landslide pixels in our dataset was systematically decreased, indicate similar model results as long as more than 250 non-landslide pixels are used. With lower non-landslide numbers, the explanatory power of the model reduces significantly and the regression coefficients become unstable. Still, the proportion of non-landslide locations versus landslides in our dataset is not representative for the true landslide/non-landslide proportion. Hence, the *LSS* values (between 0 and 1) have only a relative significance. They do not represent the relative frequency of landslide occurrences between different locations, but only indicate whether a location is less or more susceptible to landsliding compared to another location in the study area.

Univariate logistic regression analyses on this selected dataset indicate that the maximum slope (*SMA*), mean local relief (*MLR*), peak ground acceleration (*PGA*), mean annual precipitation (*P*), tree cover and dummy variables for the lithological classes unconsolidated sediments (*SU*), siliciclastic sedimentary rocks (*SS*) and volcanic rocks (*VOLC*) are significant to predict landslide occurrence, considering the Wald test statistic at the 0.01 significance level. The Rainy Day Normal and other

lithological classes, were not significant. The significant variables, except for tree cover, were used to test multiple regression models of *LSS*. Tree cover showed a positive correlation with *LSS*. Such positive relation contradicts most studies indicating that vegetation reinforces slope stability (e.g.: Gariano & Guzzetti, 2016; Glade, 2003; Guns & Vanacker, 2013; Vannoppen et al., 2016). Furthermore, this variable showed a highly significant positive correlation with precipitation ( $p \lll 0.01$ ). This intercorrelation might explain the positive relation between tree cover and *LSS*. Moreover, this positive correlation might be attributable to mapping biases. Due to the detection limit of smaller and shallow mass movements on the satellite imagery, many of the landslides in our inventory (especially those mapped in Google Earth) are deep-seated (large) landslides. For these landslides, the effect of trees on slope stability is mostly limited to increased evapotranspiration, while root reinforcement has only a minor influence (Sidle & Bogaard, 2016). In addition, land reclamation (including soil tillage and land levelling) in cultivated (non-forested) areas shortens the conservation period of smaller and shallow landslides (resulting in their relative underrepresentation), while (large) landslides under forest are often easier to detect on satellite images and can remain visible during longer periods (Guzzetti et al., 2012). For these reasons, the positive correlation between landslide occurrence and tree cover is likely spurious. It was therefore decided to exclude this variable from our further analyses.

Fig. 3 shows the explained variance of the different multiple logistic regression models that were tested. In general, all models shown in Fig. 3 indicate that the performance of the validation data (1/3) is very similar to the performance of the calibration data (2/3, i.e. 6400 points).

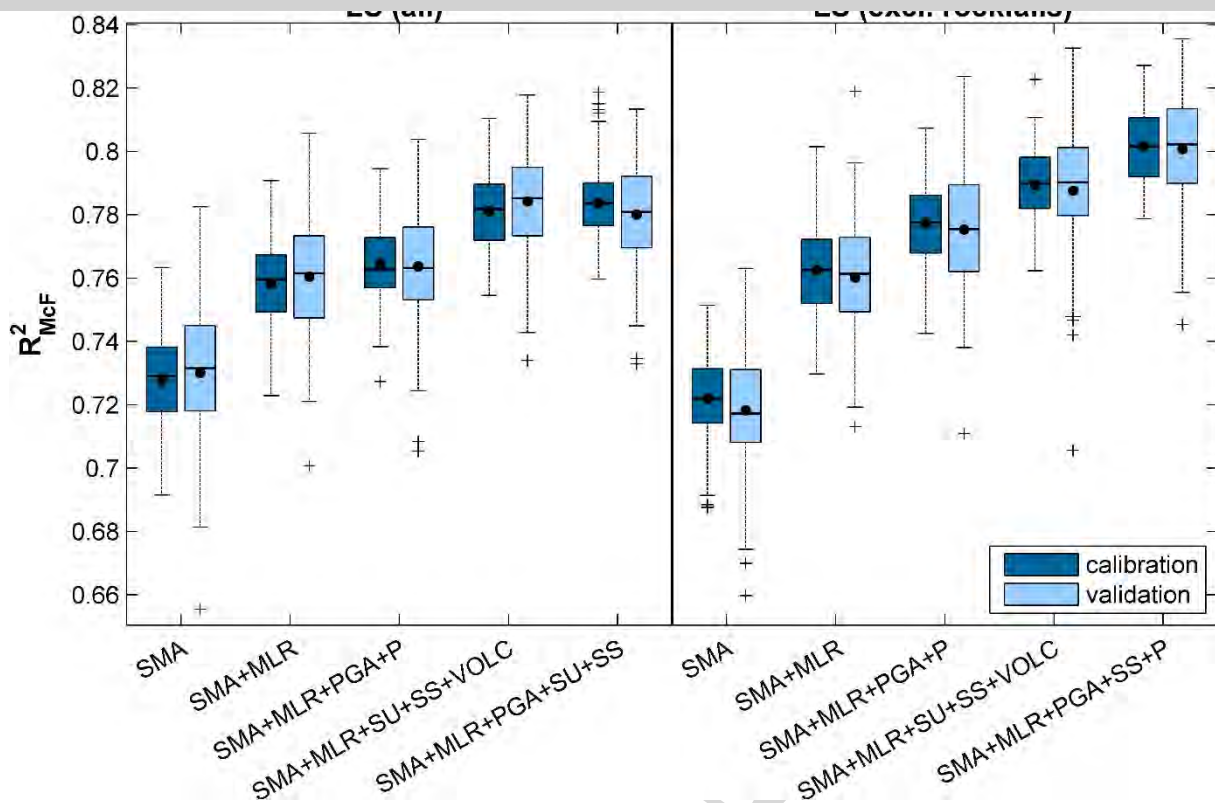


**Fig. 3.** Boxplots of the explained variance ( $R^2_{McF}$ ), for different variable combinations of 101 simulations for the model of all landslide types (left) and for the model excluding rockfalls (right). The different predictor variables are explained in Table 1. For all simulations the dataset (containing 9652 landslide and non-landslide locations) is randomly divided in a calibration (2/3) and a validation (1/3) dataset (see section 2.3).

Analysis of the factors and models displayed in Fig. 3, indicates that SMA (Fig. 4A) explains by far most of the variance in  $LSS$ . Adding  $MLR$  (Fig. 4B) significantly increases the explained variance for both the model based on all landslide types and the model excluding known rockfalls. Model performance further increases significantly when  $PGA$  (Fig. 4C) and  $P$  (Fig. 4D) are added, especially for the model excluding rockfalls, but for the model considering all landslide types,  $P$  is not significant at the 0.01 significance level ( $p = 0.01$ ). Model performance also increases when lithological variables are taken into account. Both siliciclastic sedimentary rocks and unconsolidated sediments (Fig. 4E) are significant ( $p < 0.01$ ) for the model of all landslide types. Only siliciclastic sedimentary rocks are significant, for the model excluding rockfalls.

Based on these results, a final selection of variables was made (see final pair of boxplots in Fig. 3). For both models the explained variance was significantly larger, compared to the other tested models where all predictor variables were significant at  $p = 0.01$ . Both models have topography, but also seismicity as a common basis to predict *LSS*. The fact that precipitation is not significant for the model considering all landslide types, can be explained by the presence of many rockfalls in dryer regions (e.g. the Sahara, Fig. 2). This finding also concurs with other studies, finding no or very weak correlations between rockfalls and precipitation as a trigger (Perret, 2006; Sandersen, 1997). Moreover, as explained above, the effect of vegetation might counteract the importance of precipitation as a factor in the model, due to strong intercorrelation between the two factors. The importance of this effect could not be determined and needs further research to refine large-scale susceptibility maps with more detailed (higher resolution) parameters for vegetation cover and precipitation. With respect to lithology, the class of unconsolidated sediments was not significant for the model excluding rockfalls. This lithological class covers a vast area in the Sahara and in southwest Africa (Fig. 4E). These are two dry areas, already characterized by lower susceptibilities due to the precipitation factor that is included in this model. Moreover, areas with unconsolidated sediments are typically characterized by low topographic relief (Fig. 4), while rockfalls generally occur on very steep slopes in other lithologies.

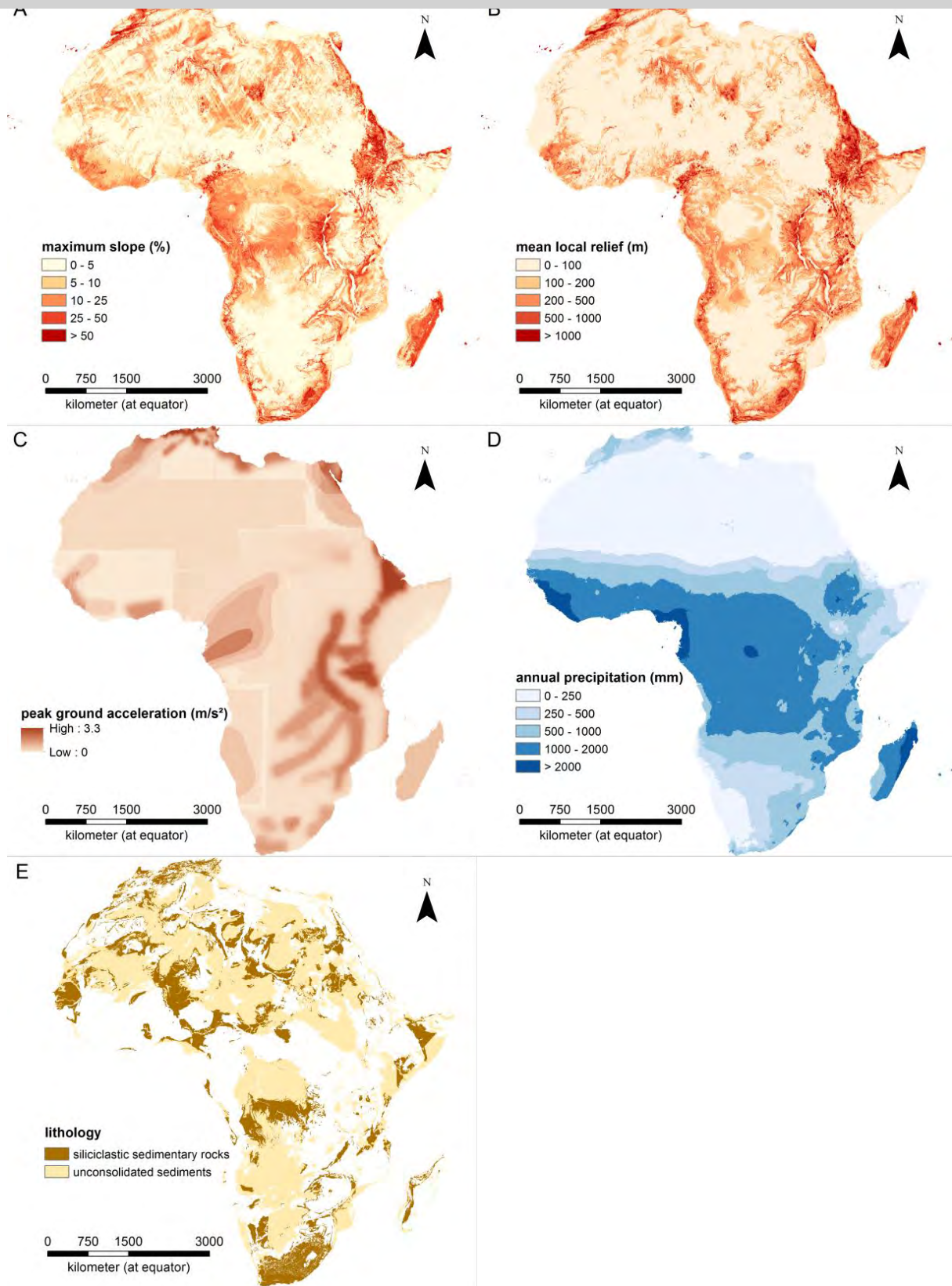


**Fig. 4. Spatial pattern of significant environmental variables in Africa, considered in the landslide susceptibility models. Data sources are given in Table 1.**

The model based on all landslide types and the model excluding known rockfalls are represented by equation 2 and 3, respectively. Both models explain about 80% of the variance in landslide occurrence.

$$p(\mathbf{y} = \mathbf{1}) = \frac{1}{1+e^{-(-4.95+0.16*SMA+0.0026*MLR+0.93*PGA-0.83*SU+1.56*SS)}} \quad \text{equation 2}$$

$$p(\mathbf{y} = \mathbf{1}) = \frac{1}{1+e^{-(-6.34+0.14*SMA+0.0033*MLR+1.12*PGA+2.06*SS+0.00099*P)}} \quad \text{equation 3}$$

The sets of regression coefficients in these equations were determined by selecting the median coefficient value of *SMA* (the most significant variable) from the 101 Monte Carlo simulations. For the other variables, we selected the coefficients corresponding to this median *SMA*. Fig. 5 shows the *ROC* curves corresponding to model equations 2 and 3. For both, the area under the *ROC* curve (*AUC*) is very high (>0.95), which indicates excellent discrimination of landslide and non-landslide pixels according to Swets (1988).

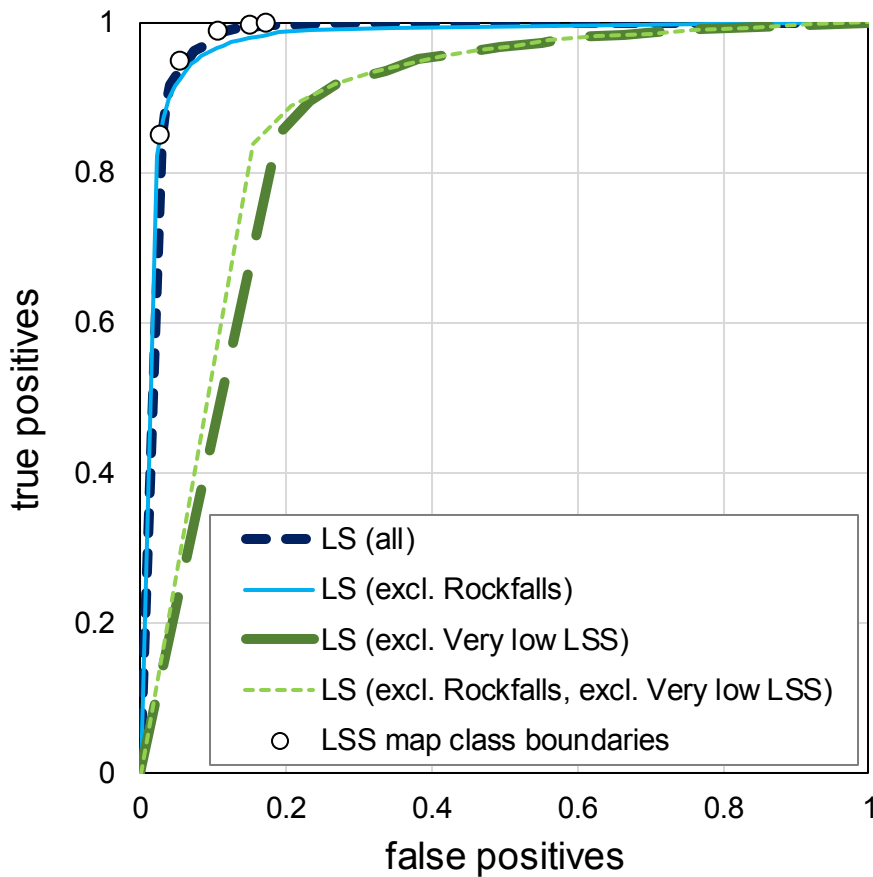


**Fig. 5.** *ROC* curves of the calibration data for the model based on all landslide types and for the model excluding rockfalls, with area under the curve (*AUC*) values of 0.98 and 0.97, respectively. The curves in green are the corresponding *ROC* curves, but excluding the lowest susceptibility class, with *AUC* values of 0.86 and 0.88 respectively. The class boundaries of the landslide susceptibility maps are shown on the *ROC* curve for the model based on all landslide types with decreasing susceptibility from left to right.

The ROC curves were used to derive the five class boundaries to reclassify the final LSS maps, presented in Fig. 6 and Fig. 7. For the model equations 2 and 3, respectively 5% and 4% of the study area was classified as having a very high susceptibility, containing respectively, 85% and 82% of all landslides used for model calibration. Respectively 95% and 93% of these landslides are located in regions with at least a high susceptibility and respectively 99% and 97% in regions with at least a moderate susceptibility. These three classes together cover about 10% of Africa. Given that almost 85% of the study area has a very low susceptibility, we constructed the same ROC curves, excluding this susceptibility class, to assess the dependence of the high AUC values on the large low susceptibility class (Fig. 5). This way, AUC values of 0.86 and 0.88 were obtained for respectively the model based on all landslide types and the model excluding rockfalls. Hence, the AUC decreased significantly, due to the removal of over 80% of the true negative values corresponding to the 'very low' susceptibility class, but remained very high. Overall, these results demonstrate the great potential of these maps for landslide risk reduction and disaster planning at continental scale as they can accurately pinpoint the regions at risk by indicating a small fraction of the total land area that contains nearly all observed landslides.

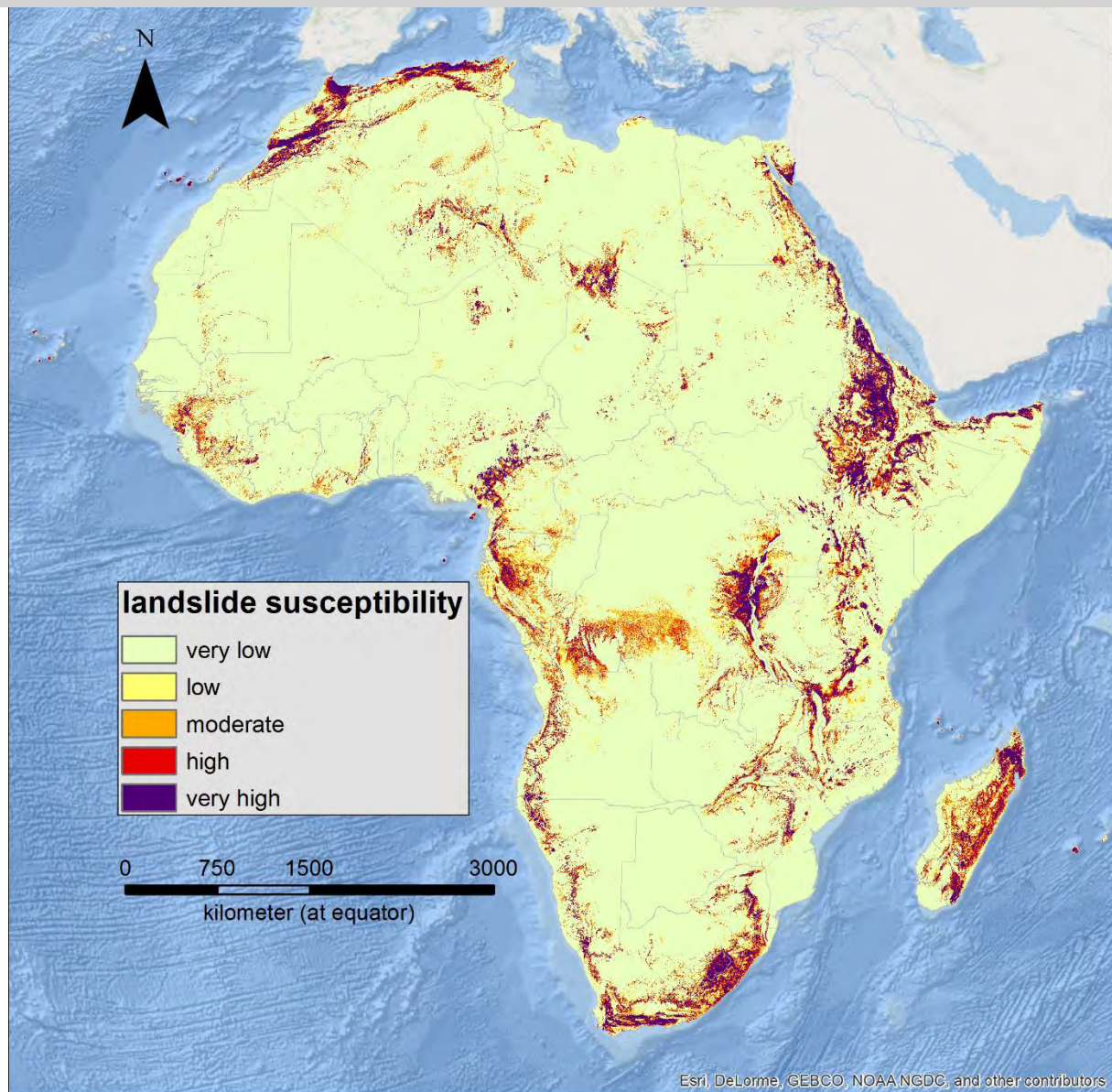


**Fig. 6. Classified landslide susceptibility map taking into account all landslide types (equation 2).**

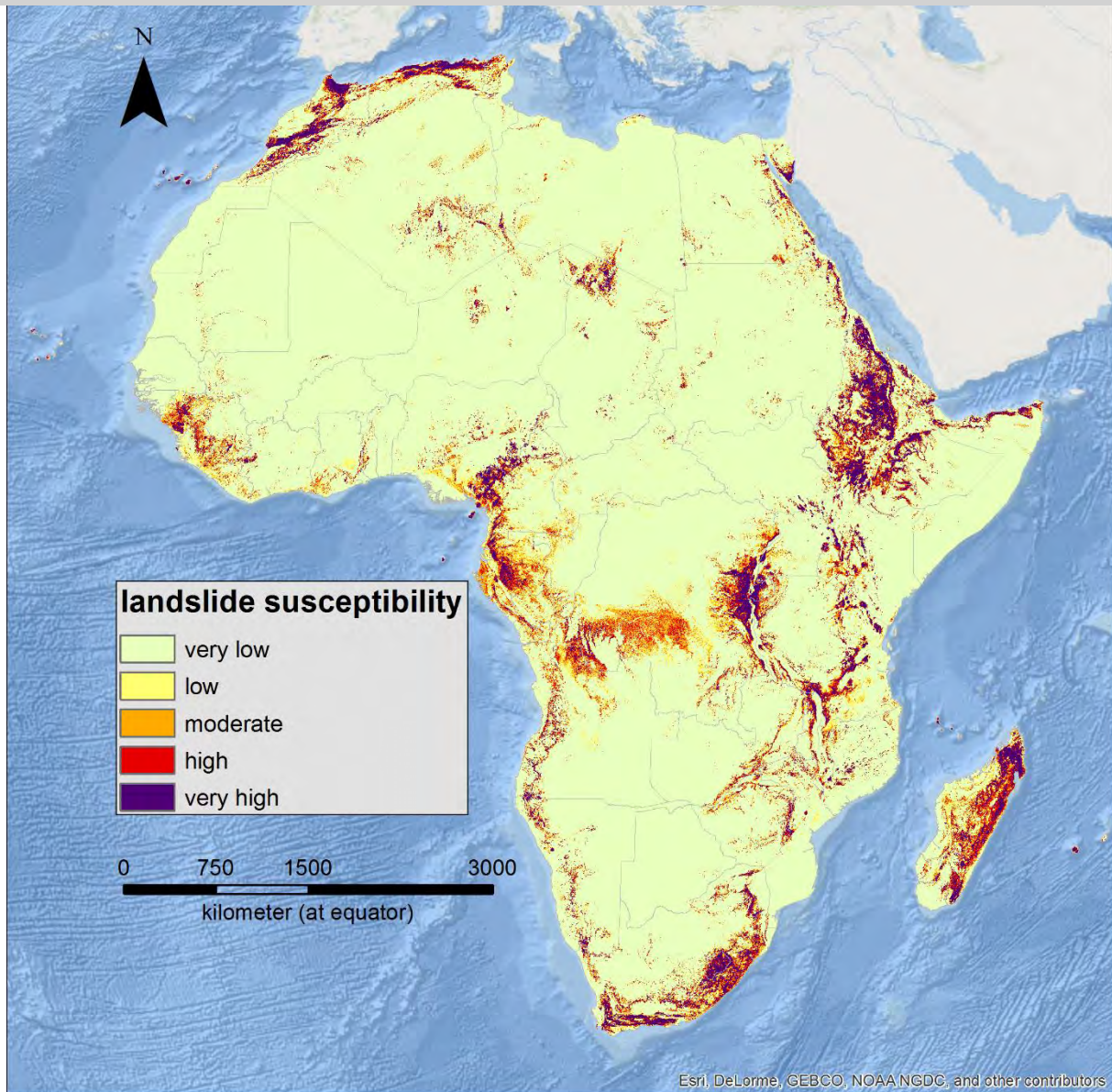


**Fig. 7. Classified landslide susceptibility map excluding known rockfalls (equation 3).**

The *LSS* maps for Africa in Fig. 6 (based on all landslide types) and Fig. 7 (excluding the known rockfalls from *LSD2* compiled in Google Earth) overall show a very similar pattern. This is mainly due to the importance of the slope gradient in both empirical models, which was also considered as a critical factor in the heuristic global *LSS* model of Stanley & Kirschbaum (2017). We must acknowledge that although rockfalls mapped in Google Earth were excluded from the second model (Fig. 7), we cannot rule out that some rockfalls are still included in the dataset compiled from the literature (*LSD1*). Nonetheless, the fraction of rockfalls in this dataset is expected to be relatively low as most studies mainly focus on other landslide types, confined to regions very prone to landsliding (Table 2). In this way, potential rockfalls in *LSD1*

are likely to be located in places affected by other types of landslides as well. Fig. 6 displays a quantitative comparison between the 10% highest *LSS* values of both models. The models agree on these high susceptibilities for 83% of the pixels (grey), but disagree on the remainder of the pixels: for each model, 8.5% of the pixels belonged to the highest 10% of the *LSS* values of that model only (green and blue). Overall, the model based on all landslide types identifies more susceptible zones in dryer regions (e.g. the Sahara), while the model excluding known rockfalls predicts that wet regions and areas with siliciclastic sedimentary rocks (e.g. West-Africa and northeast Madagascar) are more susceptible.

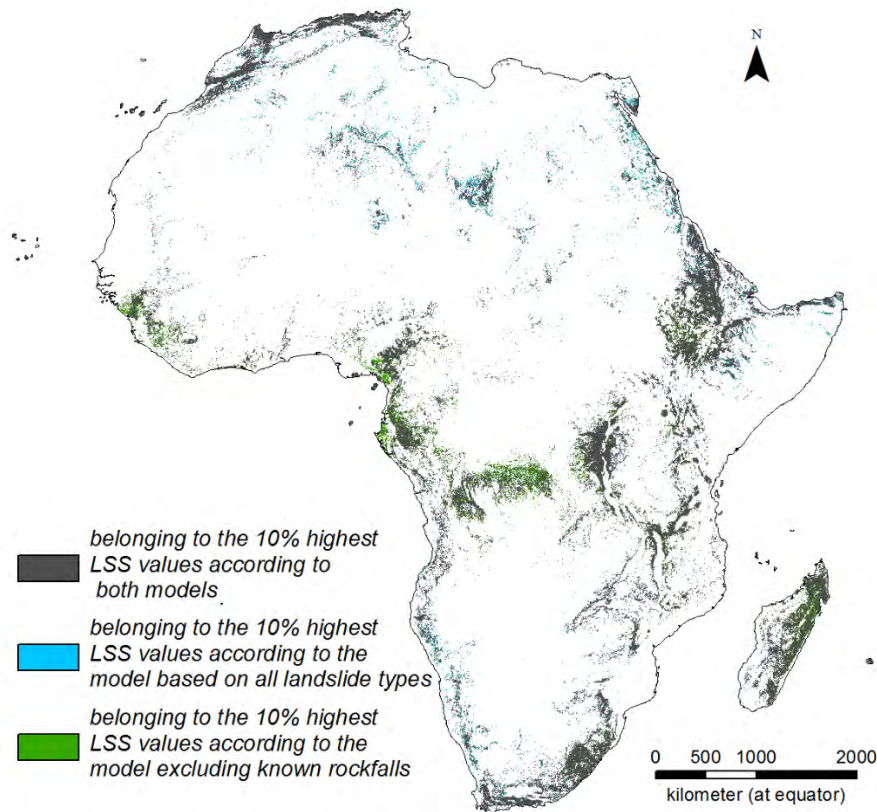


**Fig. 8. Spatial distribution of the differences in areas belonging to the 10% highest landslide susceptibility (LSS) values for the model based on all landslide types (equation 2) and the model excluding rockfalls (equation 3).**

In general both models correspond very well to the combined pattern of *SMA* (Fig. 4A) and *MLR* (Fig. 4B), with high values for both variables resulting in high *LSS*. While it can be argued that including two topographic factors is redundant, *MLR* can be considered as an important factor on its own, as it avoids assigning high *LSS* to steep slopes in areas with low local relief. This resolves problems related to artefacts in the *SMA* data (e.g. satellite tracks in the Sahara desert), but also corresponds to our understanding that areas with larger local relief are overall effectively more prone to landslide occurrence. For instance, due to larger slope length and contributing areas and due to higher uplift and rainfall rates (e.g. van Westen et al., 1997).

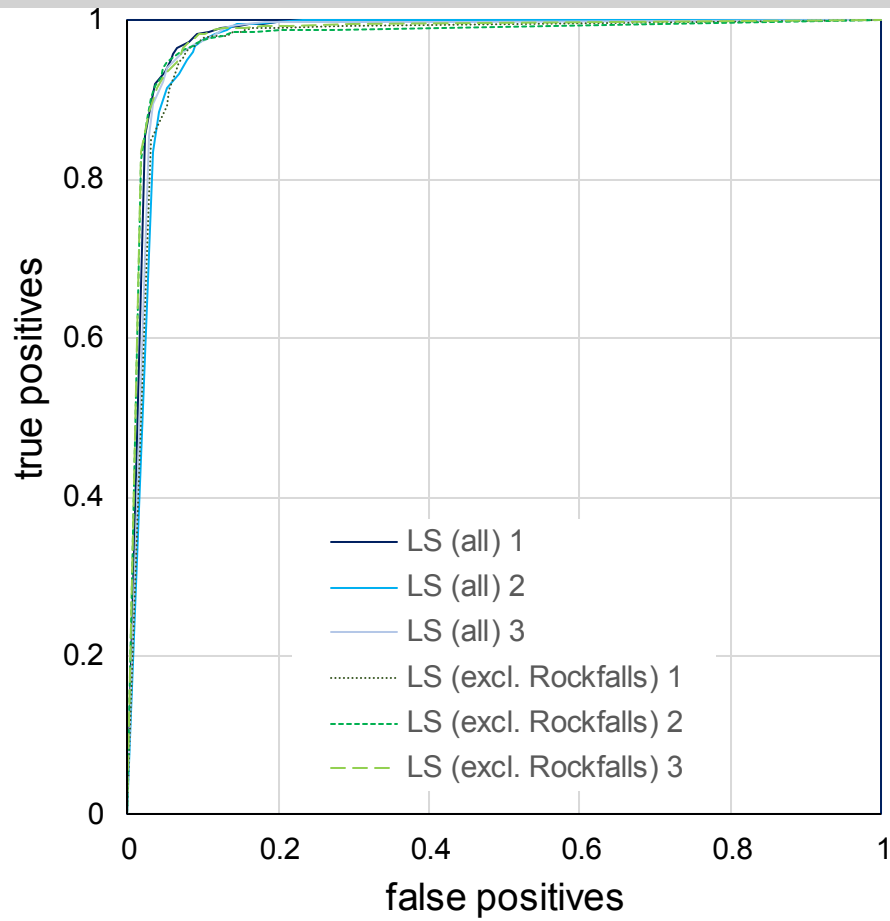
Besides topographic variables, the other significant factors seem to only have a modifying effect on *LSS* at the continental scale. The fact that *AUC* values ( $>0.95$ ) for

the model only taking into account *SMA* and *MLR* remain high, further illustrates the limited effect of the other variables on the relative *LSS* values and the general *LSS* pattern in Africa. Nonetheless, a comparison of a model taking into account only *SMA* and *MLR* with our full models indicates that *LSS* at the same location can be easily underestimated by a factor 2 to 5 and sometimes even more than 10 times in regions with high *PGA*, *P* and the occurrence of siliciclastic sedimentary rocks. This underestimation of *LSS* mainly occurs for locations with low to moderate *LSS*, while their impact on high to very high *LSS* values, foremostly determined by topography, is limited. Moreover, it is important to take these significant variables (*PGA*, *P* and lithological variables) into account in our models, due to their large impact on the absolute *LSS* values in certain regions, resulting in a more correct approximation of the actual *LSS* for the entire continent.

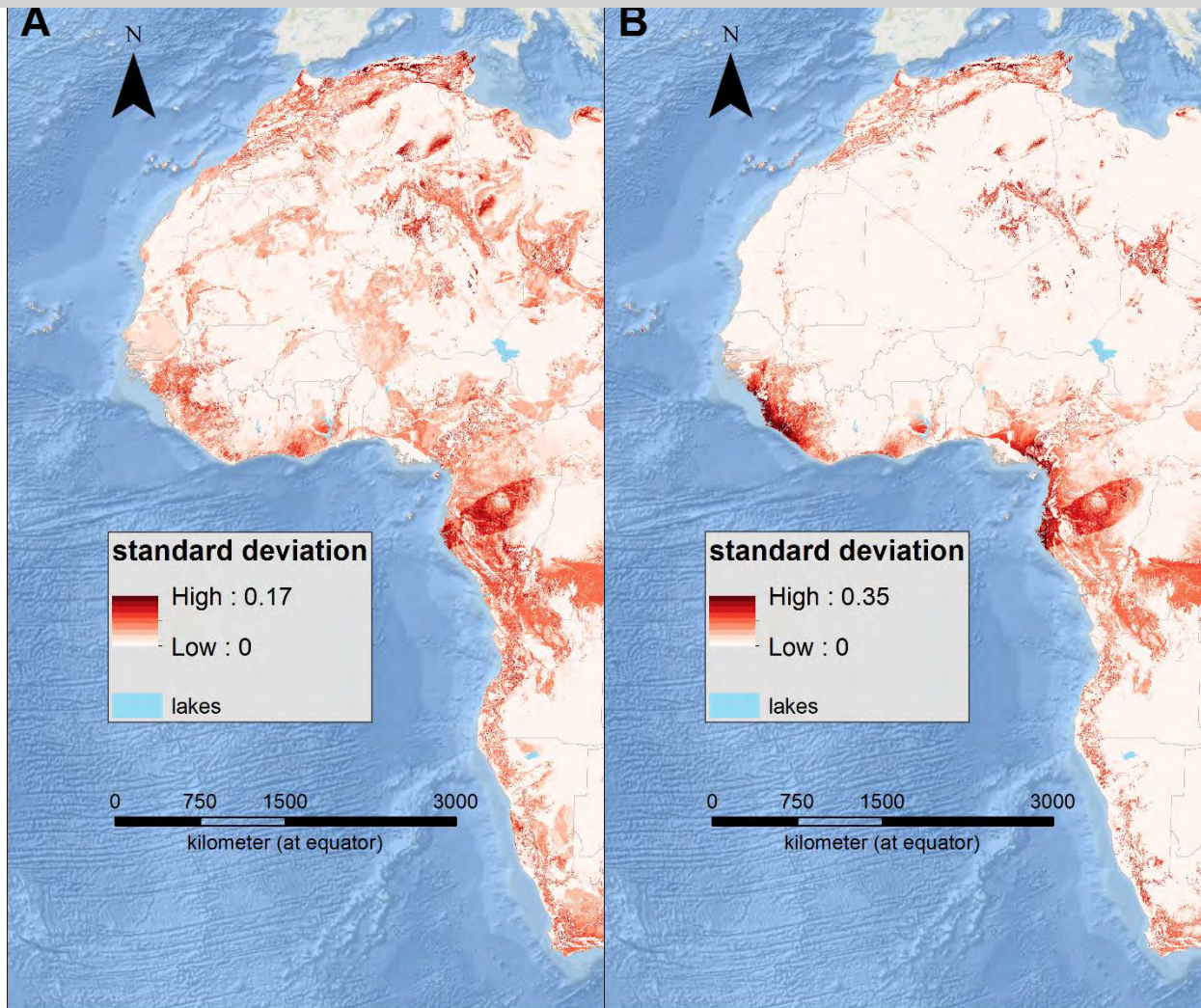
### 3.2.2. Validation and uncertainty assessment

Fig. 9 shows *ROC* curves for 6 randomly selected validation datasets from the Monte Carlo simulations (3 for both *LSS* models). The curves are very similar to those of the calibration dataset (Fig. 5), with *AUC* values that are also very high (0.97-0.98). As discussed in section 3.2.1, our two *LSS* models, were constructed based on a Monte Carlo simulation procedure using 101 different landslide subsets. This also allowed to determine the standard deviation on the *LSS* in each pixel, over all these simulations. Mapping these standard deviations provides insight into the uncertainty of the models in different regions (Fig. 10). Overall, we find that standard deviations (*std*) of *LSS* (with values between 0 and 1) are very small for both the model based on all landslide types (mean *std*: 0.009) and the model excluding known rockfalls (mean *std*: 0.012). This implies that the model results are little influenced by selecting different subsets of our calibration dataset. Nevertheless, Fig. 10 does not show a uniform pattern across Africa, with clearly higher standard deviations in some regions.

A comparison of the maps in Fig. 10 with Fig. 2 and an analysis of mean standard deviations of *LSS* at the country level demonstrates that regions having larger uncertainties are not corresponding to regions and countries with lower landslide densities in the dataset. The patterns of standard deviations are more closely linked to the considered environmental variables (Fig. 4). Uncertainties are larger in areas with high *PGA* and *P* and in places where siliciclastic sedimentary rocks are present and unconsolidated sediments are absent. The topographical factors show a more complicated pattern. Uncertainties are smaller in areas with low and high *SMA* and *MLR* and they are larger in areas with intermediate *SMA* and *MLR*. Hence, these uncertainties are not directly proportional to *LSS*. However, because of their relation to the different variables, uncertainties are generally small for the most and least susceptible areas and (although still very low) higher for areas having a moderate *LSS*. The latter areas are typically characterized by a combination of high *PGA*, high *P* or the presence of siliciclastic sedimentary rocks and low to intermediate maximum slopes (ca. 5-25%). Examples of such areas can be found along the coast of Sierra Leone and Liberia (very high *P* and low to intermediate *SMA*) or in Gabon and north-west Ethiopia (high *PGA* and intermediate *SMA*). These observations are in line with the results and discussion above: topography is the dominant factor and in case of high or low topography, model uncertainty is very low. Only for areas of intermediate relief, the interplay with other variables affects the resulting *LSS* and we observe that these variables are positively correlated with model uncertainty. This further indicates that the role of these other (non-topographic) variables is relatively harder to constrain. This is possibly because these factors can affect landslide occurrence in many ways and because their interactions can be complex. However, also the coarse resolution of available precipitation, seismicity and lithology data that was used (Table 1) and their associated uncertainties, likely play an important role here.



*Fig. 9. ROC curves for 6 randomly selected validation datasets from the Monte Carlo simulations (3 for both LSS models), with ROC values ranging between 0.97 and 0.98.*



**Fig. 10. Standard deviation of landslide susceptibility for the model with all landslide types (A) and for the model excluding rockfalls (B), based on 101 simulations.**

### 3.2.3. Potential biases linked to climate and human impacts

The African continent spans a wide variety of climates, certainly in terms of precipitation variability (Peel et al., 2007). Most landslide inventories are compiled at a local to regional scale (Guzzetti et al., 2012) and thus within one climate type. As a result, little attention has hitherto been drawn to the landslide sample bias resulting from climatic differences. Also, our Monte Carlo simulation approach discussed above does not allow to fully take this aspect into account, as the sampling of subsets remains constrained to our dataset of detected landslides.

In Fig. 11 we propose a conceptual model illustrating this potential bias. Vegetation regrowth and other geomorphic process rates (e.g. soil erosion and sediment deposition) can vary between different climates, therefore spectral signatures of landslides can accordingly last longer or shorter. Where vegetation grows rapidly and other geomorphic process rates are high, i.e. in humid tropical areas, the landslide scars can be obliterated in a matter of months or seasons. This is especially the case for small and shallow landslides. In densely populated areas, soil tillage and land levelling can accelerate this process. As a result, many smaller landslides in (sub-)humid and densely populated regions likely remain undetected. On the other hand, landslides in (semi-)arid regions can remain 'fossilized' in the landscape during centuries to millennia. Hence, one can expect that for an equal size, many landslides in dry regions (desert and steppe) are on average older than those observed in the wet tropics. Assuming that our landslide inventory reflects the occurrence of landslides over periods of decades to centuries, smaller landslides in (semi-)arid regions will be likely overrepresented. Moreover, it may well be that the

environmental conditions that triggered landslides, observed today in arid regions, may differ from the current conditions.

These differences in relative landslide representation in inventories may lead to biases in *LSS* that remain difficult to quantify. However, to explore the magnitude of this effect, we calibrated an additional *LSS* model that excluded all landslides mapped in arid regions (equation 4, Fig. 12) and compared this model with our proposed *LSS* models (Fig. 6 and Fig. 7).

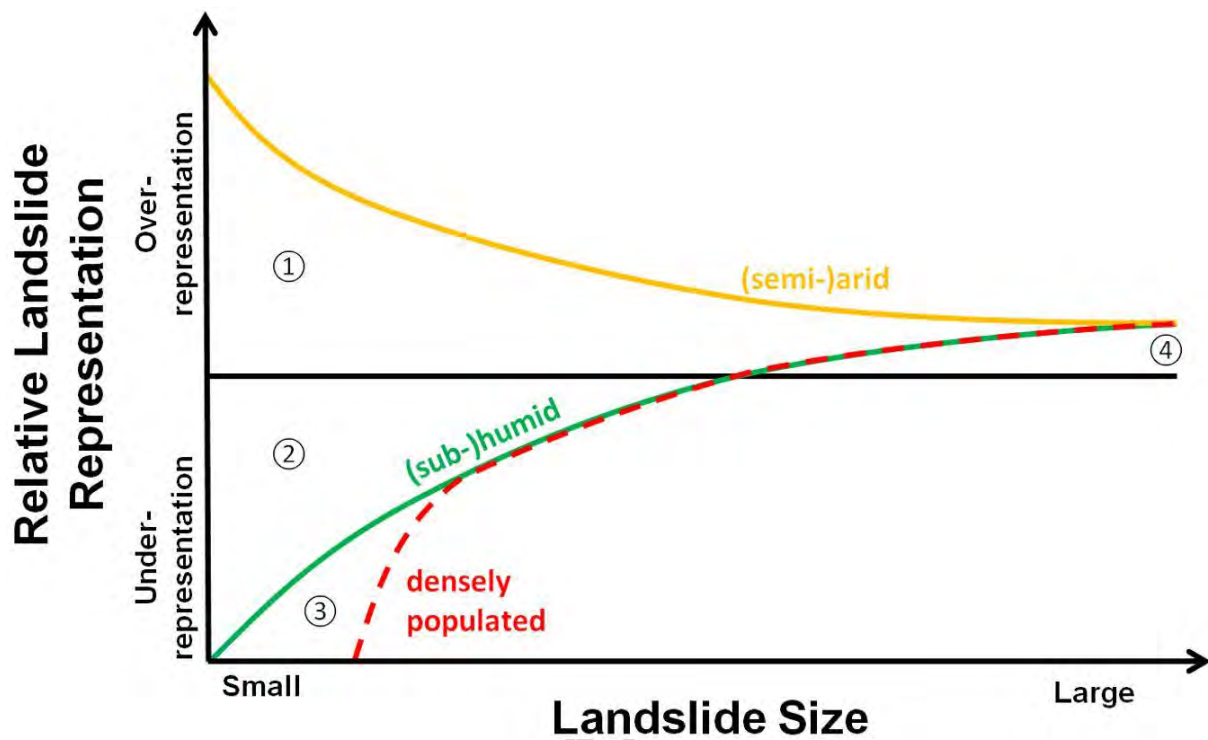


Fig. 11. Conceptual model, illustrating the effect of landslide size, climate and land use on the relative representation of landslides in a landslide inventory (based on field observations or on the analysis of remote sensing images) at the continental scale. Relative landslide representation indicates the ratio between the number of observed landslides in the inventory and the number of landslides that occurred over the past decades to centuries. (1) In arid to semi-arid regions, (especially smaller) landslides are likely over-represented because landslides that occurred over the course of millennia are likely to remain well preserved. (2) In humid and sub-humid regions, the number of smaller landslides is typically underrepresented as landslide scars are rapidly overgrown by vegetation and as other geomorphic processes (erosion and sediment deposition) may rapidly modify their morphology. (3) In densely populated areas, the underrepresentation of smaller landslides is further enhanced by human interventions (e.g. soil tillage and land levelling). (4) However, even in humid and densely populated areas, the largest landslides typically remain detectable over a long period and are therefore most likely slightly overrepresented compared to their occurrence during the past decades to centuries.

Excluding the arid climates resulted in a removal of 1870 landslides from the dataset of 7641 landslides used to calibrate the *LSS* model based on all landslide types (section 3.2.1). Logistic regression analyses resulted in the following *LSS* model (equation 4):

$$p(\mathbf{y} = \mathbf{1}) = \frac{1}{1 + e^{-(-5.99 + 0.13 * SMA + 0.0034 * MLR + 0.97 * PGA + 2.58 * SS + 0.0007 * P + 0.97 * VOLC)}} \quad \text{equation 4}$$

The environmental variables taken into account in this model are the same as those for the model excluding rockfalls, with the addition of the lithology class of volcanic rocks as a significant positive predictor variable. Also, the model coefficients for the topographic variables, the main predictors of *LSS*, are very similar. Consequently, the resulting *LSS* map excluding arid climates (Fig. 12), shows a very similar pattern to the presented *LSS* in Fig. 6 and especially Fig. 7. AUC values of the constructed ROC curves for the calibration data outside arid regions and for the excluded data inside those regions are 0.97 and 0.98, respectively. This indicates that the model performance remains very high, even for the arid regions that were excluded from the calibration. This is in line with what can be expected as topography is by far the main predictor of landslides at the continental scale in Africa.

Overall, these analyses show that the exclusion of arid climates, has a limited effect on the *LSS* pattern, mainly due to the overriding effect of topography. The main difference however, is that precipitation becomes a significant factor when arid regions are excluded. The same was the case when known rockfalls were excluded (equation 3; Fig. 7). Most of these rockfalls were indeed mapped in the Sahara

Desert. This seems to support the idea that landslides in arid regions are linked to environmental conditions that prevailed in the past and indeed points to the suggested age bias due to climatic differences (Fig. 11). However, it is also possible that the environmental conditions explaining the occurrence of recent landslides differ for arid and non-arid regions and that the dominant types of currently triggered landslides are different in both regions. Based on our observations, we believe that both hypotheses are true; (1) landslides currently observed in arid climates are on average older than landslides currently observed in humid climates and (2) landslides, likely dominantly of different types (e.g. rockfalls, flow-type landslides), are also currently triggered in dry climates (e.g. Dinis et al., 2013). As a result, it remains impossible to fully quantify the effect of potential biases in landslide representation (Fig. 11) on the resulting *LSS* at continental scale. We therefore recommend, as a scope for further research, to further explore and quantify these potential representation biases, e.g. by confronting inventories of mapped landslides with information on landslide rates for study areas in contrasting climatic zones. Such analyses may further our understanding of *LSS* patterns at large scale and especially improve hazard and risk assessment in Africa.

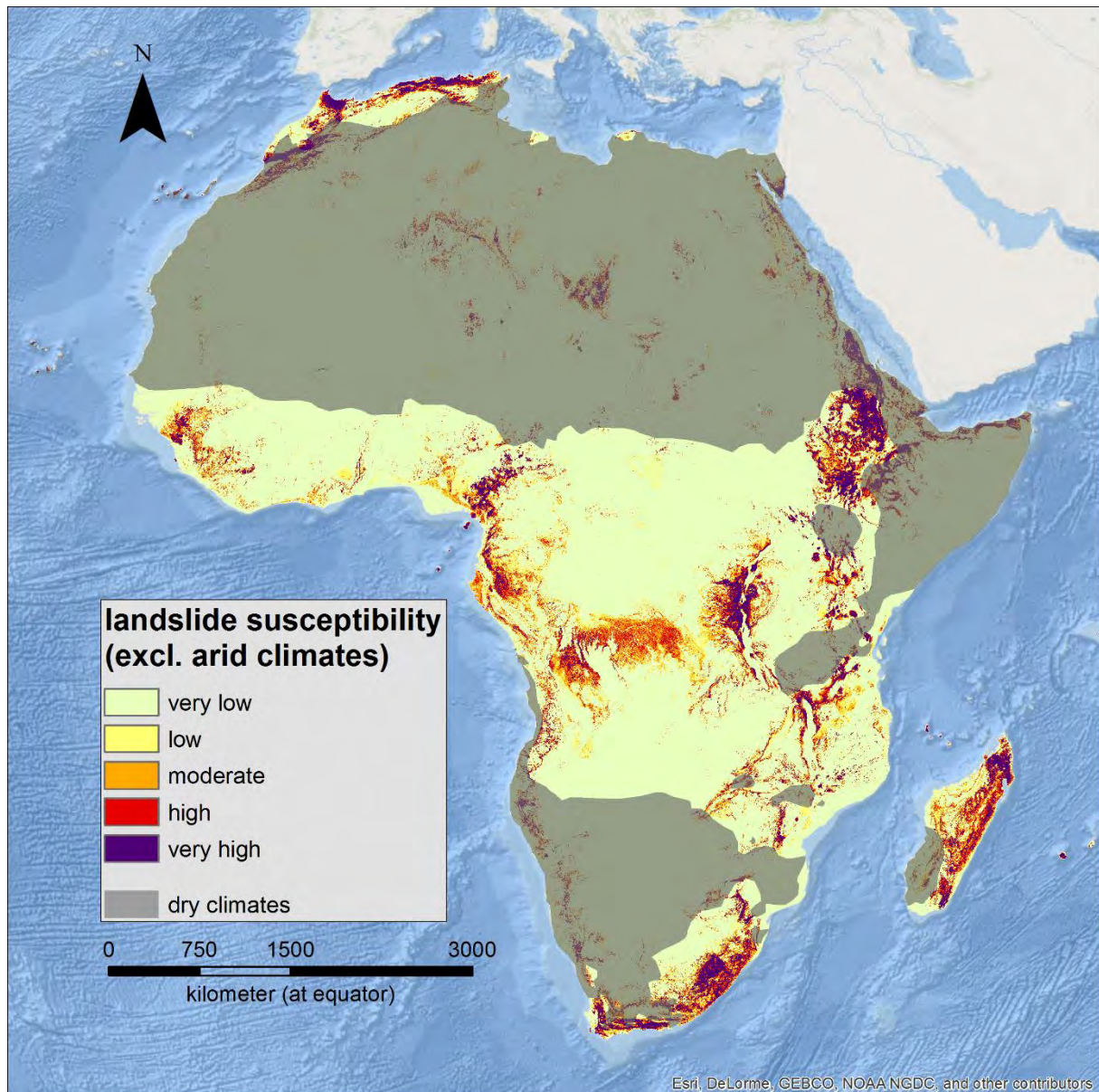


**Fig. 12.** Classified landslide susceptibility map excluding arid climates (equation 4).

### 3.2.4. Comparison with other studies on landslide susceptibility

Overall, these results are in accordance with the continental *LSS* study for Europe of Van Den Eeckhaut et al. (2012), which also indicates that topographical variables are by far the most important control on the occurrence of landslides. Like us, they also included 10 other variables (lithology, geology, soil and land cover classes) in their model to differentiate *LSS* within areas having similar topographical characteristics. However, they did not include variables relating to seismicity and precipitation, which

were both found to be significant for predicting *LSS* in Africa. While precipitation and seismicity can be considered as triggering factors of landslides (and are therefore at first sight more appropriate for landslide hazard analyses), they were included in our models because previous research clearly shows that they can also have an important impact on *LSS*. Both seismicity and precipitation can also weaken substrates and decrease soil stability (by shaking, weathering and saturation), resulting in an increased susceptibility to landsliding as well as larger landslide responses during subsequent triggering events (e.g. Broeckx et al., 2016; Chang et al., 2007; Chuang et al., 2009; Hovius et al., 2011; Molnar et al., 2007; Nowicki et al., 2014; Steger et al., 2016; Vanmaercke et al., 2017).

While we present the first *LSS* maps specifically focussing on Africa, our landslide maps can also be compared with the landslide susceptibility of Africa as presented in global *LSS* maps. Stanley & Kirschbaum (2017), Hong et al. (2007) and Nadim et al. (2006) produced such global landslide hazard and landslide susceptibility models. Their maps are not calibrated with actual landslide data, but are expert-based and provide less detail in terms of spatial resolution. Nevertheless, the general patterns of *LSS* in these maps correspond well to our models. The few regions showing moderate landslide hazard in Nadim et al. (2006) match with the highly susceptible regions around Mount Cameroon, the Ethiopian Highlands and further south along the East-African rift in our models. In the model of Hong et al. (2007) additional susceptible regions can be observed in Morocco, west Angola, east South-Africa (Lesotho), Madagascar and even the Hoggar and Tibesti Mountains in the central Sahara. This model, although very roughly, corresponds to our *LSS* models for most of the continent. The most recent model (Stanley & Kirschbaum, 2017) is also the

one that shows spatial patterns of *LSS similar* to our susceptibility models (Fig. 6 and Fig. 7) As discussed above, this is mainly due to the dominant effect of topography on *LSS*.

The results of our *LSS* maps also allow to evaluate the landslide data availability of African countries in relation to the country's *LSS* (Fig. 13). It can be observed that highly susceptible countries in general also have a relatively large number of mapped landslides in our dataset (green circles). Exceptions are Liberia, Sierra Leone and Guinea in West-Africa, Gabon and Equatorial Guinea at the west coast of Central-Africa, Zimbabwe and a number of Islands (e.g. Sao Tome and Principe, Mauritius). For these (mostly tropical) countries the quality of the Google Earth satellite imagery is often insufficient to map landslides (e.g. due to cloud cover). Likewise, our literature review revealed no studies reporting landslide data for these countries. When considering the number of landslide studies (white circles), Fig. 13 shows that countries along the East-African Rift region, North-Africa, Cameroon and South Africa are relatively well represented. However, there is a substantial share of African countries that are prone to landsliding with few to no landslide-mapping studies available. These under-researched countries include all countries listed above (e.g. Liberia, Gabon, Zimbabwe) and several smaller countries (e.g. Lesotho, Swaziland, Djibouti, Cabo Verde). However, also for several larger countries where landslides were mapped in Google Earth, relatively few landslide studies are currently available (e.g. Madagascar, Eritrea, DR Congo). Given their high susceptibility to landsliding, our results underline the need for landslide research in these countries.

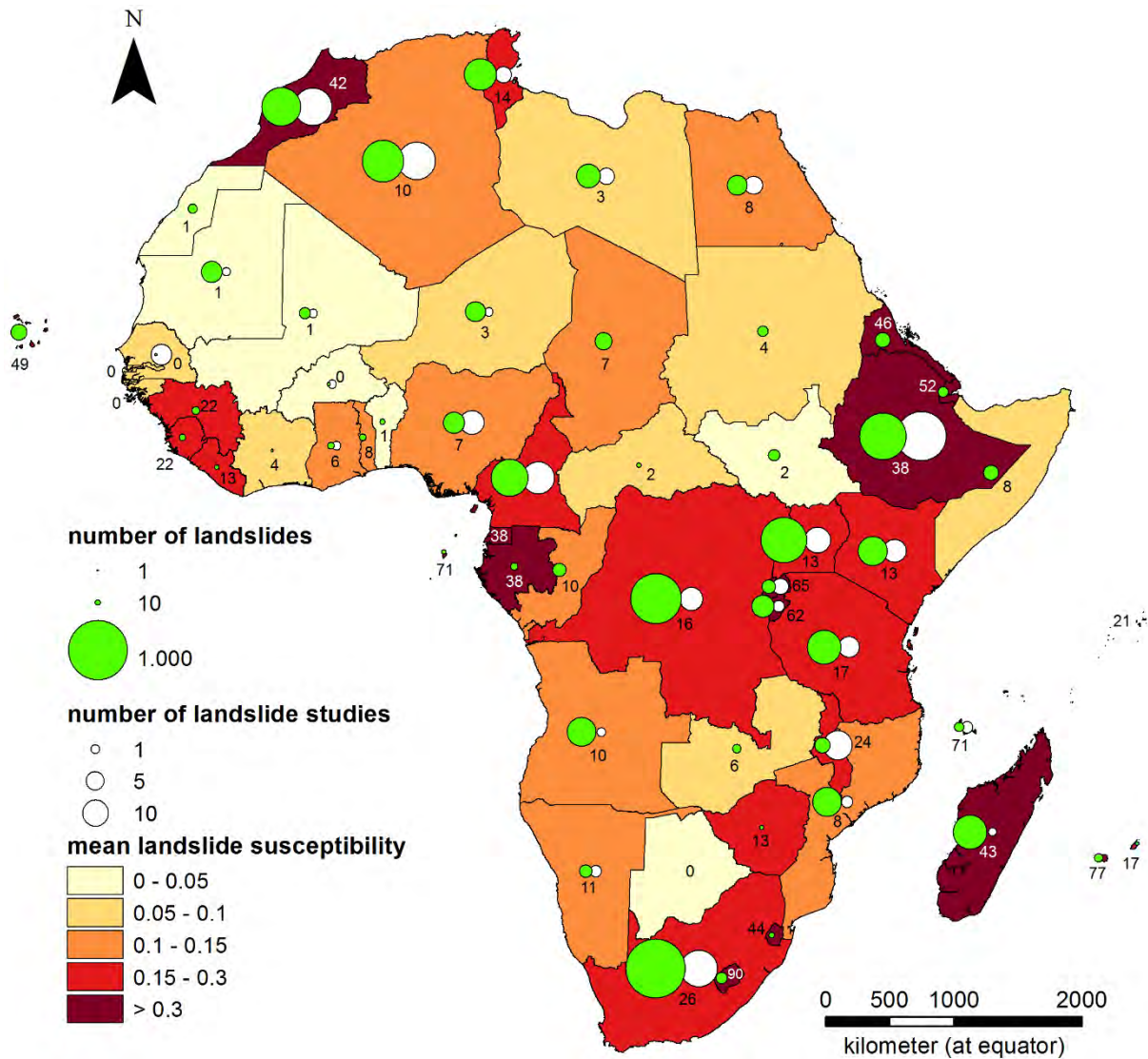


*Fig. 13: Overview by country of the number of landslides in the calibration dataset, the number of landslide studies from our literature review and the mean landslide susceptibility. Numbers indicate the areal percentage of the country with moderate to very high landslide susceptibility.*

### 3.2.5. Landslide susceptibility in Africa: scope for further research

Spatial patterns of *LSS* at the continental scale are dominantly determined by topography. However, also other factors (e.g. precipitation, lithology, seismicity) play a significant role. Their effect remains more difficult to constrain in continental-scale models. This may be due to the complex role they may play, but especially also because of the relatively crude nature of the data sources at continental scale and

their associated uncertainties. Hence, there is a need for better quality (and resolution) data on environmental variables in Africa at continental scale, to better assess their importance for *LSS*. Likewise, such data are needed for landslide hazard and risk assessments.

Improved data on potential controlling factors will also allow to better assess the many potential interactions between these factors that may affect landslide occurrence. Improved understanding and quantitation of these interactions will not only benefit *LSS* assessments at the continental scale, but also landslide hazard and risk assessments. Such interactions include the interplay between lithology, seismicity and geology that are often complex but may strongly affect the occurrence of landslides (e.g. Clarke and Burbank, 2010; Vanmaercke et al., 2017). However, also interactions between climate, vegetation and soil moisture are likely important. For instance, during exploratory analyses, we found a significantly negative correlation between mean annual air temperature and landslide occurrence, even after considering the effect of topography, seismicity, precipitation and lithology. It remains unclear to what extent this is a spurious correlation or not. Given that air temperature is generally not considered as a factor controlling *LSS* (Pourghasemi & Rossi, 2017; Reichenbach et al., 2018), we did not further consider this effect. However, we advise future researchers to further explore this effect. One potential hypothesis is that differences in mean air temperature at the continental scale might affect the water balance resulting in a significant indirect effect of air temperature on *LSS*. Comparing patterns of landsliding with modelled components of the water balance and data on soil moisture may help to clarify this.

Our data compilation and analyses further show that the available landslide inventories remain limited for Africa. At the country level, landslide densities of the compiled dataset correspond well to the mean *LSS* in these countries (Fig. 13) and the uncertainty on *LSS* is not larger in areas with smaller landslide densities. However, some countries prone to landsliding are clearly underrepresented in terms of landslide research. These include: Guinea, Sierra Leone, Liberia, Equatorial Guinea, Gabon, Eritrea, Djibouti, DR Congo, Burundi, Tanzania Zimbabwe, Swaziland, Lesotho, Madagascar, Cabo Verde, Sao Tome and Principe, the Seychelles and Mauritius. Based on our uncertainty analyses, we also recommend that future landslide mapping efforts focus on areas of intermediate topography to further constrain the *LSS* of these areas in relation to other environmental factors (e.g. lithology, seismicity, precipitation). Furthermore, there is an important need for inventories including the (approximative) age of landslides. This is not only necessary to better assess and avoid potential climatic biases in landslide susceptibility assessments (Fig. 11), but also crucial for landslide hazard and risk assessments across Africa.

### **3.3. Relation between landslide susceptibility and catchment sediment yield**

In this section we present an application of our *LSS* map, apart from its primary use as a basis for natural hazard assessment or risk management. The compilation of landslide data and resulting *LSS* maps in combination with a compilation of sediment yield (*SY*) for 500 catchments in Africa by Vanmaercke et al. (2014), provides a unique opportunity to explore the importance of landslides for *SY* at continental scale, as done by previous studies at smaller scales (e.g. Broeckx et al., 2016; Delmas et al., 2009; de Vente et al., 2006; Vanmaercke et al., 2017). More

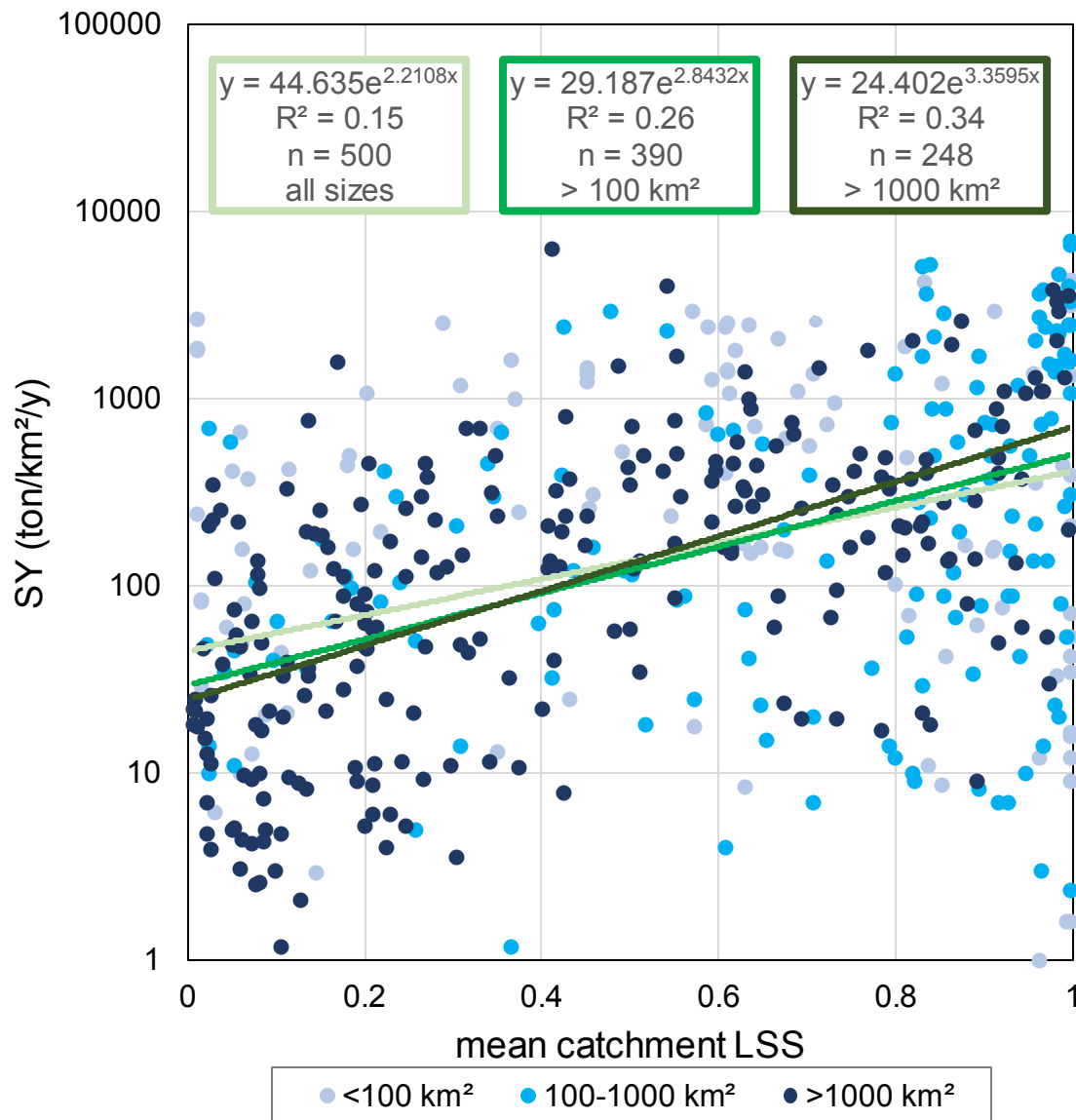
specifically, *LSS* has proven to be a significant predictor of *SY* at the regional scale, suggesting the importance of landslides to explain spatial patterns in *SY* (Broeckx et al., 2016).

Fig. 14 shows the relation between *LSS* and *SY* for Africa, for 500 catchments compiled by Vanmaercke et al. (2014). *SY* and also *LSS* tend to be smaller for larger catchments. A highly significant positive relation exists between *LSS* and *SY* and the relation further improves when only larger catchments are considered (Spearman  $R^2$  of 0.26 and 0.34 for catchments larger than 100 km<sup>2</sup> and 1000 km<sup>2</sup>, respectively). Even when considering all catchments, *LSS* explains as much of the variance ( $R^2$ : 0.15) as the best predictors for *SY* in Africa, i.e. *PGA*, *MLR* and tree cover. However, *LSS* as a single predictor for *SY* scores rather poorly compared to an integrated model constructed by Vanmaercke et al. (2014), explaining 40% of the variance. Nonetheless, a visual comparison of the modeled *SY* pattern for Africa shows an overall correspondence with our *LSS* maps (Fig. 6 and Fig. 7).

The significant positive relationship and the corresponding spatial patterns between *LSS* and *SY* suggest that landslides contribute significantly to *SY* in Africa. This strong relationship is certainly remarkable taking into account the errors on the measured *SY* data and the rough approach of using *LSS* as an approximation of actual landslide rates contributing to *SY*. On the other hand, spatial autocorrelation exists between landsliding and other erosion processes, like sheet and rill erosion and gully erosion, as could also be observed while mapping landslides in Google Earth. In this respect, despite the high incidence of landslides in a number of regions across Africa, it is still uncertain if landsliding is a dominant process determining the

variation of SY in Africa at the continental scale. This is what might be expected for a large continent with vast areas of relatively low relief. It is also in line with the limited spatial extent (10%) of the area moderately to very highly susceptible to landsliding, as predicted by our models. Further integrated research, compiling quantitative data on the different erosion processes is required to assess their relative importance as geomorphologic drivers at the continental scale for Africa.

ACCEPTED MANUSCRIPT



*Fig. 14. Mean catchment landslide susceptibility (LSS) predicted by the LSS model excluding rockfalls versus sediment yield (SY) for 500 catchments in Africa, compiled by Vanmaercke et al. (2014).*

#### 4. Conclusions

In this study a first continent-wide landslide susceptibility assessment for Africa was made, based on a landslide dataset representing the entire continent. Two separate models were constructed, one including all landslide types and one excluding

rockfalls that were mapped in Google Earth. Overall, both models show a very similar susceptibility pattern, largely determined by topography as the main predictor for landslide occurrence in both models. The other significant variables, i.e. seismicity, lithology and for the model excluding rockfalls also precipitation, have only a modifying effect on the overall pattern. Nevertheless, at regional scale landslide susceptibility can be easily underestimated by a factor 5, if these variables are not taken into account. Both models explain about 80% of the variance in landslide occurrence and successfully distinguish between landslide and non-landslide locations. Based on these models, about 10% of the African continent was assigned a moderate to very high landslide susceptibility. This area included 97-99% of all mapped landslides. Uncertainties on the *LSS* models are directly related to the predictor variables. We find the highest uncertainties for intermediate topography and areas with high precipitation and seismicity and the occurrence of siliciclastic sedimentary rocks. This points to the need for higher resolution data on these variables at the continental scale as well as the need for additional mapping efforts in such areas.

Landslide susceptibility was tested as a predictor for *SY*. The significant positive relation suggests that landslides contribute to an increased *SY* in Africa. However, the relatively low explanatory power of *LSS* suggests that landsliding is unlikely to be the single main driver of sediment production at the continental scale in Africa.

The extensive dataset compiled and published in this study can be further refined and applied in other studies for different purposes. For instance, our understanding of landslide occurrence can likely be further improved by considering more detailed

spatial and temporal data on precipitation, soil moisture, temperature, seismicity and lithology and by studying their potential interactions. However, a key limitation here is the unknown age of most landslides. Better constraining the age (and type) of known landslides is a central issue that is needed to assess and avoid potential biases in continental scale models (e.g. as a result of climatic differences, Fig. 11), but also to advance towards landslide hazard and risk assessments. In addition, particular attention is drawn to countries that we assessed to be prone to landsliding, but lacking landslide research. (e.g.: Sierra Leone, Equatorial Guinea, Eritrea, Swaziland, Madagascar; Fig. 13). These countries very likely have several landslide-prone areas with currently little or no research available.

**Acknowledgements**

M. Vanmaercke received a postdoctoral research grant from the Research Foundation Flanders (FWO).

ACCEPTED MANUSCRIPT

## Appendices

### **Appendix A. Supplementary data**

Supplementary data to this article (i.e. all landslide locations) can be found online at [insert link]

### **Appendix B. landslide susceptibility map for all landslide types**

The landslide susceptibility map for all landslide types can be found online at [insert link]

### **Appendix C. landslide susceptibility map excluding rockfalls**

The landslide susceptibility map excluding rockfalls can be found online at [insert link]

## References

- Afungang, R.N., 2015. Spatiotemporal Probabilistic Assessment of Landslide Hazard along Bamenda Mountain Region of the Cameroon Volcanic Line. University of Yaoundé I.
- Agbor, A.T., Mohammed, A.F., usman Shehu, O., Musa, N.W., Adegbe, M., others, 2014. The October 13, 2010 Landslides on the Azenge Mountain in Imande Ukusu, Nkomon District, Benue State, Nigeria. *Environ. Ecol. Res.* 2, 113–121. doi:10.13189/eer.2014.020301
- Allison, P., 2012. Logistic regression for rare events, *Statistical Horizons*.
- Arnous, M.O., 2011. Integrated remote sensing and GIS techniques for landslide hazard zonation: A case study Wadi Watier area, South Sinai, Egypt. *J. Coast. Conserv.* 15, 477–497. doi:10.1007/s11852-010-0137-9
- Asfaw, Y.E., 2010. Landslide Assessment in Blue Nile Gorge, Central Ethiopia. Ghent University and Vrije Universiteit Brussel.
- Asma, D., 2013. Landslides in and sediment production from the Gilgel Gibe catchment, SW Ethiopia. KU Leuven and Vrije Universiteit Brussel.
- Audru, J.C., Bitri, A., Desprats, J.F., Dominique, P., Eucher, G., Hachim, S., Jossot, O., Mathon, C., Nédellec, J.L., Sabourault, P., Sedan, O., Stollsteiner, P., Terrier-Sedan, M., 2010. Major natural hazards in a tropical volcanic island: A review for Mayotte Island, Comoros archipelago, Indian Ocean. *Eng. Geol.* 114, 364–381. doi:10.1016/j.enggeo.2010.05.014
- Ayalew, L., Yamagishi, H., 2005. The application of GIS-based logistic regression for landslide susceptibility mapping in the Kakuda-Yahiko Mountains, Central Japan.

- Geomorphology 65, 15–31. doi:10.1016/j.geomorph.2004.06.010
- Ayonghe, S.N., Mafany, G.T., Ntasin, E., Samalang, P., 1999. Seismically activated swarm of landslides, tension cracks, and a rockfall after heavy rainfall in Bafaka, Cameroon. *Nat. Hazards* 19, 13–27. doi:10.1023/A:1008041205256
- Ayonghe, S.N., Ntasin, E.B., Samalang, P., Suh, C.E., 2004. The June 27, 2001 landslide on volcanic cones in Limbe, Mount Cameroon, West Africa. *J. African Earth Sci.* 39, 435–439. doi:10.1016/j.jafrearsci.2004.07.022
- Bălțeanu, D., Chendeș, V., Sima, M., Enciu, P., 2010. A country-wide spatial assessment of landslide susceptibility in Romania. *Geomorphology* 124, 102–112. doi:10.1016/j.geomorph.2010.03.005
- Bijker, H.J., 2001. A hydrological-slope stability model for shallow landslide prediction in the Injisuthi Valley, KwaZulu-Natal Drakensberg. University of Pretoria.
- Bomans, K., 2005. Spatial and temporal analysis of factors controlling landslides on the Makonde and Rondo plateaux, Southeastern Tanzania. KU Leuven.
- Bonvallot, J., 1984. Glissements de terrain et aménagement du milieu naturel dans une montagne méditerranéenne humide. Le cas des Atatfa, Kroumirie, Tunisie Septentrionale.
- Bouhadad, Y., Benhamouche, A., Bourenane, H., Ouali, A.A., Chikh, M., Guessoum, N., 2010. The Laalam (Algeria) damaging landslide triggered by a moderate earthquake ( $M_w = 5.2$ ). *Nat. Hazards* 54, 261–272. doi:10.1007/s11069-009-9466-0
- Bourenane, H., Bouhadad, Y., Guettouche, M.S., Braham, M., 2015. GIS-based landslide susceptibility zonation using bivariate statistical and expert approaches

- in the city of Constantine (Northeast Algeria). *Bull. Eng. Geol. Environ.* 74, 337–355. doi:10.1007/s10064-014-0616-6
- Broeckx, J., Vanmaercke, M., Balteanu, D., Chendes, V., Sima, M., Enciu, P., Poesen, J., 2016. Linking landslide susceptibility to sediment yield at regional scale: application to Romania. *Geomorphology* 268. doi:10.1016/j.geomorph.2016.06.012
- Broeckx, J. et al., in prep. Landslide susceptibility and rates in the Mt Elgon region, Uganda.
- Broothaerts, N., Kissi, E., Poesen, J., Van Rompaey, A., Getahun, K., Van Ranst, E., Diels, J., 2012. Spatial patterns, causes and consequences of landslides in the Gilgel Gibe catchment, SW Ethiopia. *Catena* 97, 127–136. doi:10.1016/j.catena.2012.05.011
- Budimir, M.E.A., Atkinson, P.M., Lewis, G.G., 2015. A systematic review of landslide probability mapping using logistic regression. *Landslides* 12, 419–436. doi:10.1007/s10346-014-0550-5
- Busche, D., 2001. Early Quaternary landslides of the Sahara and their significance for geomorphic and climatic history. *J. Arid Environ.* 49, 429–448. doi:10.1006/jare.2001.0802
- Cameron, A.C., Windmeijer, A.G.F., 1997. An R-squared measure of goodness of fit for some common nonlinear regression models. *J. Econom.* 77, 329–342. doi:10.1016/S0304-4076(96)01818-0
- Capot-Rey, R., 1954. Crevasses sismiques et glissements de terrain en Algérie. In: *Bulletin de l'Association de géographes français* N°245-246, 31e année, Novembre-décembre 1954, 166–171.

- Chang, K.T., Chiang, S.H., Hsu, M.L., 2007. Modeling typhoon- and earthquake-induced landslides in a mountainous watershed using logistic regression. *Geomorphology* 89, 335–347. doi:10.1016/j.geomorph.2006.12.011
- Che, V.B., 2011. Slope stability analysis and landslide susceptibility assessment on the SE foot slopes of Mt Cameroon. Ghent University.
- Chiliza, S.G., Richardson, S., 2008. Landslide Incidence in the Limpopo Province, South Africa, in: *Proceedings of the First World Landslide Forum United Nations University, Tokyo, Japan*. pp. 100–103.
- Choubert, G., Ennadifi, Y., 1970. Carte géologique du flanc sud de l'anti-Atlas occidental et des plaines du Dra. Akka-Tafagout-Tata. Rabat (Morocco): Division de la Géologie.
- Chuang, S.C., Chen, H., Lin, G.W., Lin, C.W., Chang, C.P., 2009. Increase in basin sediment yield from landslides in storms following major seismic disturbance. *Eng. Geol.* 103, 59–65. doi:10.1016/j.enggeo.2008.08.001
- Clarke, B.A., Burbank, D.W., 2010. Bedrock fracturing, threshold hillslopes, and limits to the magnitude of bedrock landslides. *Earth Planet. Sci. Lett.* 297, 577–586. doi:10.1016/j.epsl.2010.07.011
- Dai, F.C., Lee, C.F., 2002. Landslide characteristics and slope instability modeling using GIS, Lantau Island, Hong Kong. *Geomorphology* 42, 213–228. doi:10.1016/S0169-555X(01)00087-3
- De Lemos, H.J., 2013. A critical analysis using remote sensing and GIS techniques for spatial distribution and macro- morphological analyses of rockfalls in the Golden Gate Highlands National Park, South Africa. University of the Witwatersrand.

- de Vente, J., Poesen, J., Bazzoffi, P., Van Rompaey, A., Verstraeten, G., 2006. Predicting catchment sediment yield in mediterranean environments: The importance of sediment sources and connectivity in Italian drainage basins. *Earth Surf. Process. Landforms* 31, 1017–1034. doi:10.1002/esp.1305
- de Vente, J., Poesen, J., Verstraeten, G., Govers, G., Vanmaercke, M., Van Rompaey, A., Arabkhedri, M., Boix-Fayos, C., 2013. Predicting soil erosion and sediment yield at regional scales: Where do we stand? *Earth-Science Rev.* 127, 16–29. doi:10.1016/j.earscirev.2013.08.014
- DeFries, R.S., Hansen, M.C., Townshend, J.R.G., Janetos, a C., Loveland, T.R., 2000. A new global 1 km dataset of percentage tree cover derived from remote sensing. *Glob. Chang. Biol.* 6, 247–254.
- Delmas, M., Cerdan, O., Mouchel, J.M., Garcin, M., 2009. A method for developing a large-scale sediment yield index for European river basins. *J. Soils Sediments* 9, 613–626. doi:10.1007/s11368-009-0126-5
- Dilley, M., 2005. Natural disaster hotspots: a global risk analysis. The World Bank, Washington DC.
- Dimanche, P., Hamza, A., 1978. Carte de l'érosion du nord et du centre de la Tunisie. Echelle : 1 : 200.000. Ministère de l'Agriculture, République Tunisienne.
- Dinis, P.A., Mantas, V., Andrade, P.S., Tonecas, J., Kapula, E., Pereira, A., Carvalho, F.S., 2013. Contribution of TRMM rainfall data to the study of natural systems and risk assessment. Cases of application in SW Angola. *Estud. do Quaternário* 9, 33–43.
- Emam, A., El-Fakharani, A.H.S., Felesteen, A.W., Selim, S.A., Hafez, K.M., 2010. Catastrophic movement of rocks and proposed solutions to avoid its risks in the

abu el-reesh area, northeast aswan city, egypt. Arab. J. Geosci. 5, 607–616.

doi:10.1007/s12517-010-0201-7

Fonseca, A., 2014. Large deep-seated landslides in the northern Rif Mountains

(Northern Morocco): inventory and analysis. Universidade de Lisboa.

Gabert, P., 1984. Séismes , néotectonique et effets induits sur les versants des

massifs des Babors dans la région de Kerrata (Algérie), In: Méditerranée,

Troisième série, Tome 51, 1-2-1984. Actes du colloque <<Effets des séismes

sur les reliefs de forte énergie>>, 25–31.

Gariano, S.L., Guzzetti, F., 2016. Landslides in a changing climate. Earth-Science

Rev. 162, 227–252. doi:10.1016/j.earscirev.2016.08.011

Gerland, P., Raftery, a. E., Ev lkova, H., Li, N., Gu, D., Spoorenberg, T., Alkema, L.,

Fosdick, B.K., Chunn, J., Lalic, N., Bay, G., Buettner, T., Heilig, G.K., Wilmoth,

J., 2014. World population stabilization unlikely this century. Science (80-. ). 346,

234–237. doi:10.1126/science.1257469

Giardini, D., Grünthal, G., Shedlock, K.M., Zhang, P., 1999. The GSHAP Global

Seismic Hazard Map. Ann. Di Geofis. 42, 1225–1230.

Girma, F., 2010. A multi method approach to study landslide hazard; A case study in

Ada Berga Woreda, Western Showa Zone, Oromiya Region, Ethiopia. Addis

Ababa University.

Glade, T., 2003. Landslide occurrence as a response to land use change: A review of

evidence from New Zealand. Catena 51, 297–314. doi:10.1016/S0341-

8162(02)00170-4

Guha-Sapir, D., Below, R., Hoyois, P., 2017. The CRED/OFDA International Disaster

Database, Université Catholique de Louvain - Brussels - Belgium, EM-DAT  
www.emdat.be/database (accessed on January 11, 2017).

- Guns, M., Vanacker, V., 2013. Forest cover change trajectories and their impact on landslide occurrence in the tropical Andes. *Environ. Earth Sci.* 70, 2941–2952. doi:10.1007/s12665-013-2352-9
- Gupta, V., 2001. Geomorphological Controls on Landslide Activity in the Du Toits Kloof, Western Cape Mountains, South Africa. *South African Geogr. J.* 83, 258–262. doi:10.1080/03736245.2001.9713744
- Guzzetti, F., Mondini, A.C., Cardinali, M., Fiorucci, F., Santangelo, M., Chang, K.T., 2012. Landslide inventory maps: New tools for an old problem. *Earth-Science Rev.* 112, 42–66. doi:10.1016/j.earscirev.2012.02.001
- Hadji, R., Boumazbeur, A. errahmane, Limani, Y., Baghem, M., Chouabi, A. el M., Demdoun, A., 2013. Geologic, topographic and climatic controls in landslide hazard assessment using GIS modeling: A case study of Souk Ahras region, NE Algeria. *Quat. Int.* 302, 224–237. doi:10.1016/j.quaint.2012.11.027
- Hagos, A.A., 2012. Remote sensing and GIS-based mapping on landslide phenomena and landslide susceptibility evaluation of Debresina Area (Ethiopia) and Rio San Girolamo basin (Sardinia). Università degli Studi di Cagliari.
- Haque, U., Blum, P., da Silva, P.F., Andersen, P., Pilz, J., Chalov, S.R., Malet, J.P., Auflic, M.J., Andres, N., Poyiadji, E., Lamas, P.C., Zhang, W., Peshevski, I., Pétursson, H.G., Kurt, T., Dobrev, N., Garcia-Davalillo, J.C., Halkia, M., Ferri, S., Gaprindashvili, G., Engström, J., Keellings, D., 2016. Fatal landslides in Europe. *Landslides* 1–10. doi:10.1007/s10346-016-0689-3
- Hardwick, D., 2012. A mass movement classification for the southern Drakensberg,

South Africa. University of the Witwatersrand.

Hartmann, J., Moosdorf, N., 2012. The new global lithological map database GLiM: A representation of rock properties at the Earth surface. *Geochemistry, Geophys. Geosystems* 13, 1–37. doi:10.1029/2012GC004370

Hong, Y., Adler, R., Huffman, G., 2007. Use of satellite remote sensing data in the mapping of global landslide susceptibility. *Nat. Hazards* 43, 245–256.

doi:10.1007/s11069-006-9104-z

Hovius, N., Meunier, P., Lin, C.W., Chen, H., Chen, Y.G., Dadson, S., Horng, M.J., Lines, M., 2011. Prolonged seismically induced erosion and the mass balance of a large earthquake. *Earth Planet. Sci. Lett.* 304, 347–355.

doi:10.1016/j.epsl.2011.02.005

Igwe, O., Fukuoka, H., 2014. The effect of water-saturation on the stability of problematic slopes at the Iva Valley area, Southeast Nigeria. *Arab. J. Geosci.*

doi:10.1007/s12517-014-1398-7

Ismail, H.E.D., 2013. Regional geomorphic analysis and GIS susceptibility mapping of landslides in the Blue Nile and the Tekeze River Basins of Ethiopia. Missouri University of Science and Technology.

Jacobs, L., Dewitte, O., Poesen, J., Delvaux, D., Thiery, W., Kervyn, M., 2016. The Rwenzori Mountains, a landslide-prone region? *Landslides* 13, 519–536.

doi:10.1007/s10346-015-0582-5

Jacobs, L., Dewitte, O., Poesen, J., Maes, J., Mertens, K., Sekajugo, J., Kervyn, M., 2017. Landslide characteristics and spatial distribution in the Rwenzori Mountains, Uganda. *J. African Earth Sci.* 134, 917–930.

doi:10.1016/j.jafrearsci.2016.05.013

- Kimaro, D.N., Poesen, J., Deckers, J.A., Msita, H.B., 2010. Magnitude and severity of channel irrigation-induced landslides on different cultivation systems in the vegetable growing area of the Uluguru mountains, Tanzania, in: Nardali, E.T. (Ed.), *No-Till Farming: Effects on Soil, Pros and Cons and Potential. Agriculture Issues and Policies Series*. Nova Science Publishers, Inc., pp. 129–144.
- King, G., Zeng, L., 2001. Logistic Regression in Rare Events Data. *Polit. Anal.* 9, 137–163. doi:10.1162/00208180152507597
- Kirschbaum, D., Stanley, T., Zhou, Y., 2015. Spatial and temporal analysis of a global landslide catalog. *Geomorphology* 249, 4–15. doi:10.1016/j.geomorph.2015.03.016
- Kirschbaum, D.B., Adler, R., Hong, Y., Hill, S., Lerner-Lam, A., 2010. A global landslide catalog for hazard applications: Method, results, and limitations. *Nat. Hazards* 52, 561–575. doi:10.1007/s11069-009-9401-4
- Kirschbaum, D.B., Adler, R., Hong, Y., Lerner-Lam, a., 2009. Evaluation of a preliminary satellite-based landslide hazard algorithm using global landslide inventories. *Nat. Hazards Earth Syst. Sci.* 9, 673–686. doi:10.5194/nhess-9-673-2009
- Kjekstad, O., Highland, L., 2009. Economic and Social Impacts of Landslides, in: *Landslides-Disaster Risk Reduction*. Springer Berlin Heidelberg, pp. 573–587. doi:10.1007/978-3-540-69970-5
- Kleinbaum, D.G., Klein, M., 2010. *Logistic regression: a self-learning text*, 3rd ed. Springer-Verlag New York. doi:10.1007/978-1-4419-1742-3
- Knapen, A., Kitutu, M.G., Poesen, J., Breugelmans, W., Deckers, J., Muwanga, a., 2006. Landslides in a densely populated county at the footslopes of Mount Elgon

- (Uganda): Characteristics and causal factors. *Geomorphology* 73, 149–165.  
doi:10.1016/j.geomorph.2005.07.004
- Korup, O., Hayakawa, Y., Codilean, A.T., Matsushi, Y., Saito, H., Oguchi, T.,  
Matsuzaki, H., 2014. Japan's sediment flux to the Pacific Ocean revisited. *Earth-  
Science Rev.* 135, 1–16. doi:10.1016/j.earscirev.2014.03.004
- Maertens, M., 2016. Landslide susceptibility mapping for the Mt Elgon Region,  
Uganda. KU Leuven and Vrije Universiteit Brussel.
- Maes, J., Kervyn, M., de Hontheim, A., Dewitte, O., Jacobs, L., Mertens, K.,  
Vanmaercke, M., Vranken, L., Poesen, J., 2017. Landslide risk reduction  
measures: A review of practices and challenges for the tropics. *Prog. Phys.  
Geogr.* 41, 191–221. doi:10.1177/0309133316689344
- Maina-Gichaba, C., Kipseba, E.K., Masibo, M., 2013. Kenya: A Natural Outlook -  
Geo-Environmental Resources and Hazards. *Dev. Earth Surf. Process.* 16, 293–  
314. doi:10.1016/B978-0-444-59559-1.00010-4
- Maki Mateso, J.M., Dewitte, O., 2014. Vers un inventaire des glissements de terrain  
et des éléments à risque sur les versants du Rift à l'ouest du lac Kivu (RDC).  
*Geo. Eco. Trop.* 38, 137–154.
- Mansour, Z., Miloud, B., Donzé, F., Soraya, R., Abderahmane, H., 2014.  
Morphometric analysis of landslides in the Ouarsenis area (west Algeria):  
implications for establishing a relationship between tectonic, geomorphologic,  
and hydraulic indexes. *Arab. J. Geosci.* doi:10.1007/s12517-014-1711-5
- Marc, O., Hovius, N., Meunier, P., Uchida, T., Hayashi, S., 2015. Transient changes  
of landslide rates after earthquakes. *Geology* 43, 883–886.  
doi:10.1130/G36961.1

- Moeyersons, J., 2003. The topographic thresholds of hillslope incisions in southwestern Rwanda. *Catena* 50, 381–400. doi:10.1016/S0341-8162(01)00177-1
- Moeyersons, J., Tréfois, P., Lavreau, J., Alimasi, D., Badriyo, I., Mitima, B., Mundala, M., Munganga, D.O., Nahimana, L., 2004. A geomorphological assessment of landslide origin at Bukavu, Democratic Republic of the Congo. *Eng. Geol.* 72, 73–87. doi:10.1016/j.enggeo.2003.06.003
- Moeyersons, J., Trefois, P., Nahimana, L., Ilunga, L., Vandecasteele, I., Byizigiro, V., Sadiki, S., 2010. River and landslide dynamics on the western Tanganyika rift border, Uvira, D.R. Congo: Diachronic observations and a GIS inventory of traces of extreme geomorphologic activity. *Nat. Hazards* 53, 291–311. doi:10.1007/s11069-009-9430-z
- Molnar, P., Anderson, R.S., Anderson, S.P., 2007. Tectonics, fracturing of rock, and erosion. *J. Geophys. Res. Earth Surf.* 112, 1–12. doi:10.1029/2005JF000433
- Msilimba, G.G., 2010. The socioeconomic and environmental effects of the 2003 landslides in the Rumphi and Ntcheu Districts (Malawi). *Nat. Hazards* 53, 347–360. doi:10.1007/s11069-009-9437-5
- Msilimba, G.G., Holmes, P.J., 2010. Landslides in the Rumphi District of Northern Malawi: Characteristics and mechanisms of generation. *Nat. Hazards* 54, 657–677. doi:10.1007/s11069-009-9495-8
- Nadim, F., Kjekstad, O., Peduzzi, P., Herold, C., Jaedicke, C., 2006. Global landslide and avalanche hotspots. *Landslides* 3, 159–173. doi:10.1007/s10346-006-0036-1
- Ndyanabo, S., Vandecasteele, I., Moeyersons, J., Trefois, P., Ozer, A., 2011.

Vulnerability mapping for sustainable hazard mitigation in the city of Bukavu ,  
South Kivu DR Congo Presentation outline.

New, M., Lister, D., Hulme, M., Makin, I., 2002. A high-resolution data set of surface  
climate over global land areas. *Clim. Res.* 21, 1–25. doi:10.3354/cr021001

Ngatcha, B.N., Ekodeck, G.E., Mpele, M., Ntana, P.E., 2011. Hydrological and  
geotechnical investigations of mass movements in an equatorial city (Yaoundé,  
Cameroon). *Environ. Earth Sci.* 62, 1733–1747. doi:10.1007/s12665-010-0654-8

Ngecu, W.M., Mathu, E.M., 1999. The El-Nino-triggered landslides and their  
socioeconomic impact on Kenya. *Environ. Geol.* 38, 277–284.  
doi:10.1007/s002540050425

Ngole, V.M., Georges-Ivo, E.E., Ayonghe, S.N., 2007. Physico-chemical ,  
mineralogical and chemical considerations in understanding the 2001 Mabeta  
New Layout landslide , Cameroon. *J. Appl. Sci. Environ. Manag.* 11, 201–208.

Nibigira, L., Draidia, S., Havenith, H., 2013. La vallée du rift est-africain face aux  
risques gravitaires: cas de Bujumbura (Burundi). *Troisièmes Journées Aléas  
Gravitaires*, 2013 Sep 17-18, Grenoble (France).

Nowicki, M.A., Wald, D.J., Hamburger, M.W., Hearne, M., Thompson, E.M., 2014.  
Development of a globally applicable model for near real-time prediction of  
seismically induced landslides. *Eng. Geol.* 173, 54–65.  
doi:10.1016/j.enggeo.2014.02.002

Okagbue, C.O., 1994. Classification and distribution of recent historic landslides in  
southern Nigeria. *Eng. Geol.* 37, 263–270. doi:10.1016/0013-7952(94)90060-4

Ostaficzuk, S., 1973. Large-scale landslides in north-western Libya. *acta Geol. Pol.*

23.

Peel, M.C., Finlayson, B.L., McMahon, T.A., 2007. Updated world map of the Köppen-Geiger climate classification. *Hydrol. Earth Syst. Sci.* doi:10.5194/hess-11-1633-2007

Perret, S., Stoffel, M., Kienholz, H., 2006. Spatial and temporal rockfall activity in a forest stand in the Swiss Prealps - A dendrogeomorphological case study. *Geomorphology* 74, 219–231. doi:10.1016/j.geomorph.2005.08.009

Petley, D., 2012. Global patterns of loss of life from landslides. *Geology* 40, 927–930. doi:10.1130/G33217.1

Pontius, R.G., Schneider, L.C., 2001. Land-cover change model validation by an ROC method for the Ipswich watershed, Massachusetts, USA. *Agric. Ecosyst. Environ.* 85, 191–203. doi:doi:10.1016/S0167-8809(01)00183-9

Pourghasemi, H.R., Rossi, M., 2017. Landslide susceptibility modeling in a landslide prone area in Mazandarn Province, north of Iran: a comparison between GLM, GAM, MARS, and M-AHP methods. *Theor. Appl. Climatol.* 1–25. doi:10.1007/s00704-016-1919-2

Pradhan, B., 2013. A comparative study on the predictive ability of the decision tree, support vector machine and neuro-fuzzy models in landslide susceptibility mapping using GIS. *Comput. Geosci.* 51, 350–365. doi:10.1016/j.cageo.2012.08.023

Ramasiarinoro, V.J., Andrianaivo, L., Rasolomanana, E., 2012. Landslides and associated mass movements events in the eastern part of Madagascar : risk assessment , land use planning , mitigation measures and further strategies. *Madamines* 4, 28–41.

- Raunet, M., 1973. Région d'El Omaria. Carte morpho-pédologique.
- Reichenbach, P., Rossi, M., Malamud, B., Mihir, M., Guzzetti, F., 2018. A review of statistically-based landslide susceptibility models, *Earth-Science Reviews*. Elsevier B.V. doi:10.1016/j.earscirev.2018.03.001
- Royal Museum for Central Africa, 2016. The Natural Disaster Database for Central Africa, <http://www.africamuseum.be/collections/browsecollections/naturalsciences/earth/hazard> (accessed on September 6, 2016).
- Sahani, M., 2012. Le contexte urbain et climatique des risques hydrologiques de la ville de Butembo (Nord-Kivu /RDC). Université de Liège.
- Sandersen, F., Bakkehoi, S., Hestnes, E., Lied, K., 1997. The influence of meteorological factors on the initiation of debris flows, rockfalls, rockslides and rockmass stability. *Publ. - Norges Geotek. Inst.* 201, 97–114.
- Sassa, K., Canuti, P. (Eds.), 2009. Landslides-disaster risk reduction. Springer Berlin Heidelberg.
- Shedlock, Kaye, M., Giardini, D., Grünthal, G., Zhang, P., 2000. The GSHAP Global Seismic Hazard Map. *Seismol. Res. Lett.* 71, 679–686.
- Shongwe, M.E., van Oldenborgh, G.J., van den Hurk, B., van Aalst, M., 2011. Projected changes in mean and extreme precipitation in Africa under global warming. Part II: East Africa. *J. Clim.* 24, 3718–3733.  
doi:10.1175/2010JCLI2883.1
- Side, R.C., Bogaard, T.A., 2016. Dynamic earth system and ecological controls of rainfall-initiated landslides. *Earth-Science Rev.* 159, 275–291.  
doi:10.1016/j.earscirev.2016.05.013
- Singh, R., 2009. Landslide classification, characterization and susceptibility modeling in KwaZulu-Natal. University of the

Witwatersrand.

Souverijns, N., Thiery, W., Demuzere, M., Lipzig, N.P.M. Van, 2016. Drivers of future changes in East African precipitation. *Environ. Res. Lett.* 11, 1–27.

doi:10.1088/1748-9326/11/11/114011

Stanley, T., Kirschbaum, D.B., 2017. A heuristic approach to global landslide susceptibility mapping. *Nat. Hazards*. doi:10.1007/s11069-017-2757-y

Steger, S., Brenning, A., Bell, R., Petschko, H., Glade, T., 2016. Exploring discrepancies between quantitative validation results and the geomorphic plausibility of statistical landslide susceptibility maps. *Geomorphology* 262, 8–23.

doi:10.1016/j.geomorph.2016.03.015

Suyum, G.M., 2011. Landslide mapping assessment using GIS techniques in Dessia area, Northern Ethiopia. Ghent University and Vrije Universiteit Brussel.

Swets, J.A., 1988. Measuring the accuracy of diagnostic systems. *Science* 240, 1285–1293. doi:10.1126/science.3287615

Temesgen, B., Mohammed, M.U., Korme, T., 2001. Natural hazard assessment using GIS and remote sensing methods, with particular reference to the landslides in the Wondogenet area, Ethiopia. *Phys. Chem. Earth, Part C Solar, Terr. Planet. Sci.* 26, 665–675. doi:10.1016/S1464-1917(01)00065-4

Temple, P.H., Rapp, A., 1972. Landslides in the Mgeta Area, Western Uluguru Mountains, Tanzania. *Geogr. Ann. Ser. A Phys. Geogr.* 54, 157–193.

Thiery, W., Davin, E.L., Seneviratne, S.I., Bedka, K., Lhermitte, S., van Lipzig, N.P.M., 2016. Hazardous thunderstorm intensification over Lake Victoria. *Nat. Commun.* 7:12786, 1–15. doi:10.1038/ncomms12786

doi:10.1038/ncomms12786

- Tyoda, Z., Kemp, J., Engelbrecht, J., 2012. First results from landslide susceptibility modeling in the Western Cape Province, South Africa, in: *Proceedings of GISSA Ukubazana 2012. Muldersdrift (South Africa): EE Publishers.*
- Van Den Eeckhaut, M., Hervás, J., Jaedicke, C., Malet, J.P., Montanarella, L., Nadim, F., 2012. Statistical modelling of Europe-wide landslide susceptibility using limited landslide inventory data. *Landslides* 9, 357–369.  
doi:10.1007/s10346-011-0299-z
- Van Den Eeckhaut, M., Marre, A., Poesen, J., 2010. Comparison of two landslide susceptibility assessments in the Champagne-Ardenne region (France). *Geomorphology* 115, 141–155. doi:10.1016/j.geomorph.2009.09.042
- Van Den Eeckhaut, M., Moeyersons, J., Nyssen, J., Abraha, A., Poesen, J., Haile, M., Deckers, J., 2009a. Spatial patterns of old, deep-seated landslides: A case-study in the northern Ethiopian highlands. *Geomorphology* 105, 239–252.  
doi:10.1016/j.geomorph.2008.09.027
- Van Den Eeckhaut, M., Reichenbach, P., Guzzetti, F., Rossi, M., Poesen, J., 2009b. Combined landslide inventory and susceptibility assessment based on different mapping units: an example from the Flemish Ardennes, Belgium. *Nat. Hazards Earth Syst. Sci.* 9, 507–521. doi:10.5194/nhess-9-507-2009
- Van Den Eeckhaut, M., Vanwalleghem, T., Poesen, J., Govers, G., Verstraeten, G., Vandekerckhove, L., 2006. Prediction of landslide susceptibility using rare events logistic regression: A case-study in the Flemish Ardennes (Belgium). *Geomorphology* 76, 392–410. doi:10.1016/j.geomorph.2005.12.003
- van Westen, C.J., Rengers, N., Terlien, M.T.J., Soeters, R., 1997. Prediction of the occurrence of slope instability phenomena through GIS-based hazard zonation.

Geol. Rundschau 86, 404–414. doi:10.1007/s005310050149

Vanacker, V., Vanderschaeghe, M., Govers, G., Willems, E., Poesen, J., Deckers, J., De Bievre, B., 2003. Linking hydrological, infinite slope stability and land-use change models through GIS for assessing the impact of deforestation on slope stability in high Andean watersheds. *Geomorphology* 52, 299–315. doi:10.1016/S0169-555X(02)00263-5

Vanmaercke, M., Ardizzone, F., Rossi, M., Guzzetti, F., 2017. Exploring the effects of seismicity on landslides and catchment sediment yield: An Italian case study. *Geomorphology* 278, 171–183. doi:10.1016/j.geomorph.2016.11.010

Vanmaercke, M., Poesen, J., Broeckx, J., Nyssen, J., 2014. Sediment yield in Africa. *Earth-Science Rev.* 136, 350–368. doi:10.1016/j.earscirev.2014.06.004

Vannoppen, W., Poesen, J., Peeters, P., De Baets, S., Vandevorde, B., 2016. Root properties of vegetation communities and their impact on the erosion resistance of river dikes. *Earth Surf. Process. Landforms* 41, 2038–2046. doi:10.1002/esp.3970

Vercammen, J., 2011. Towards a landslide susceptibility map for the Gilgel Gibe catchment (Southern Ethiopia). KU Leuven and Vrije Universiteit Brussels.

Zogning, A., Ngouanet, C., Tiafack, O., 2007. The catastrophic geomorphological processes in humid tropical Africa: A case study of the recent landslide disasters in Cameroon. *Sediment. Geol.* 199, 13–27. doi:10.1016/j.sedgeo.2006.03.030



Figure 1

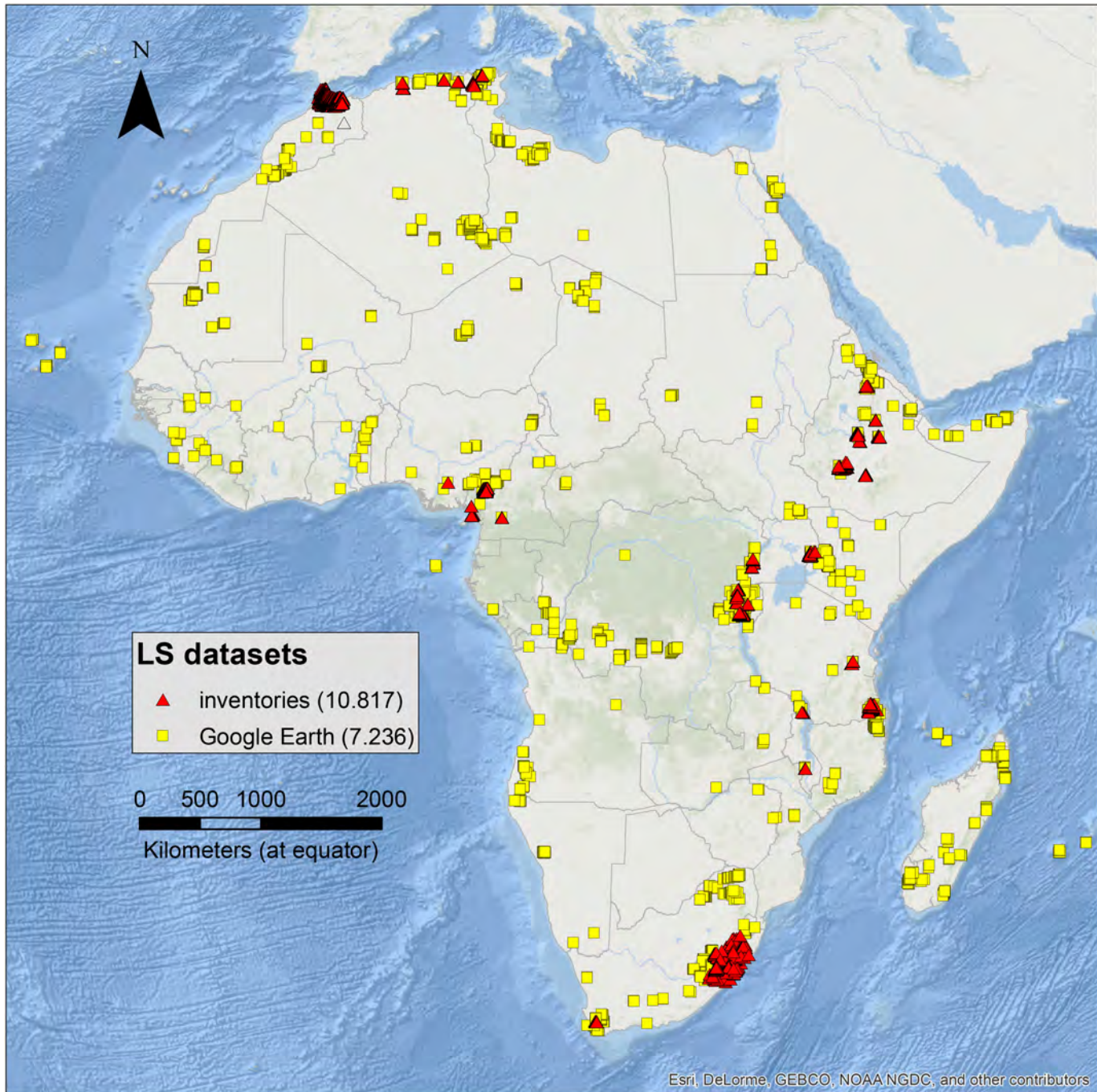


Figure 2

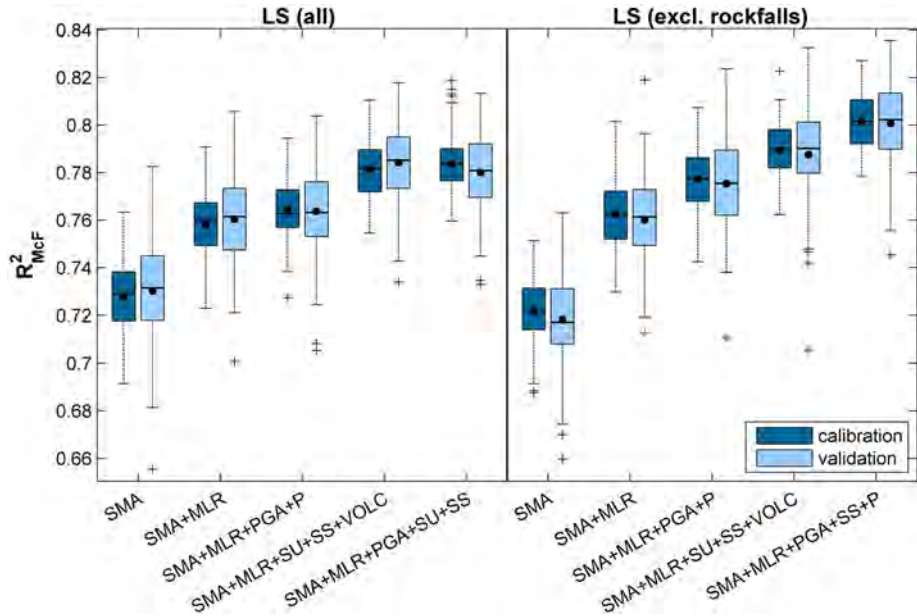


Figure 3

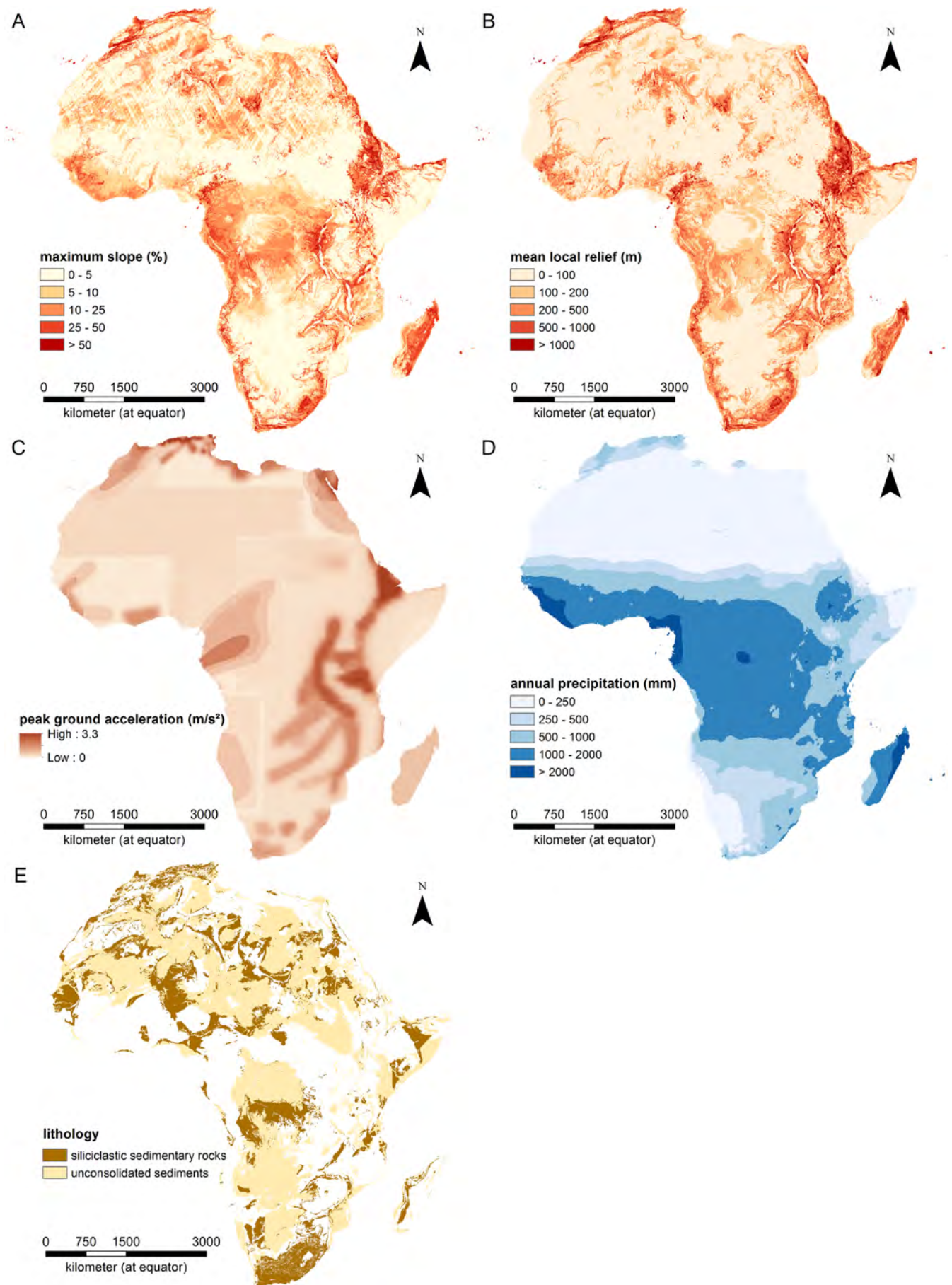


Figure 4

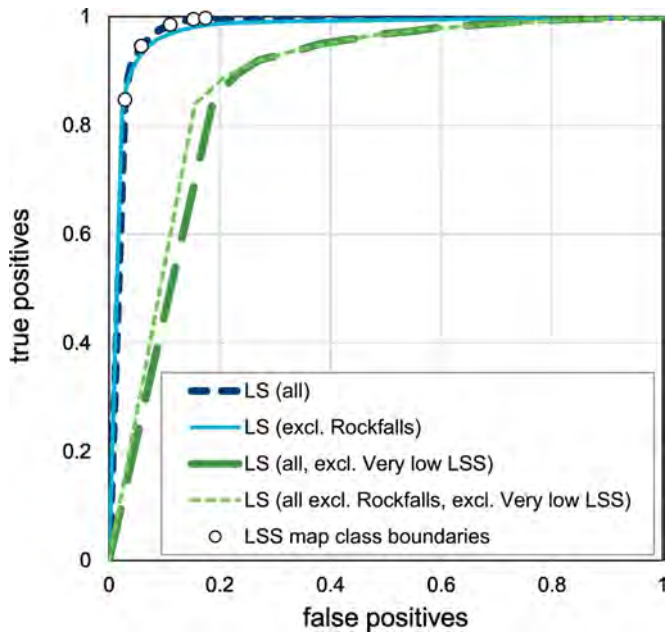


Figure 5

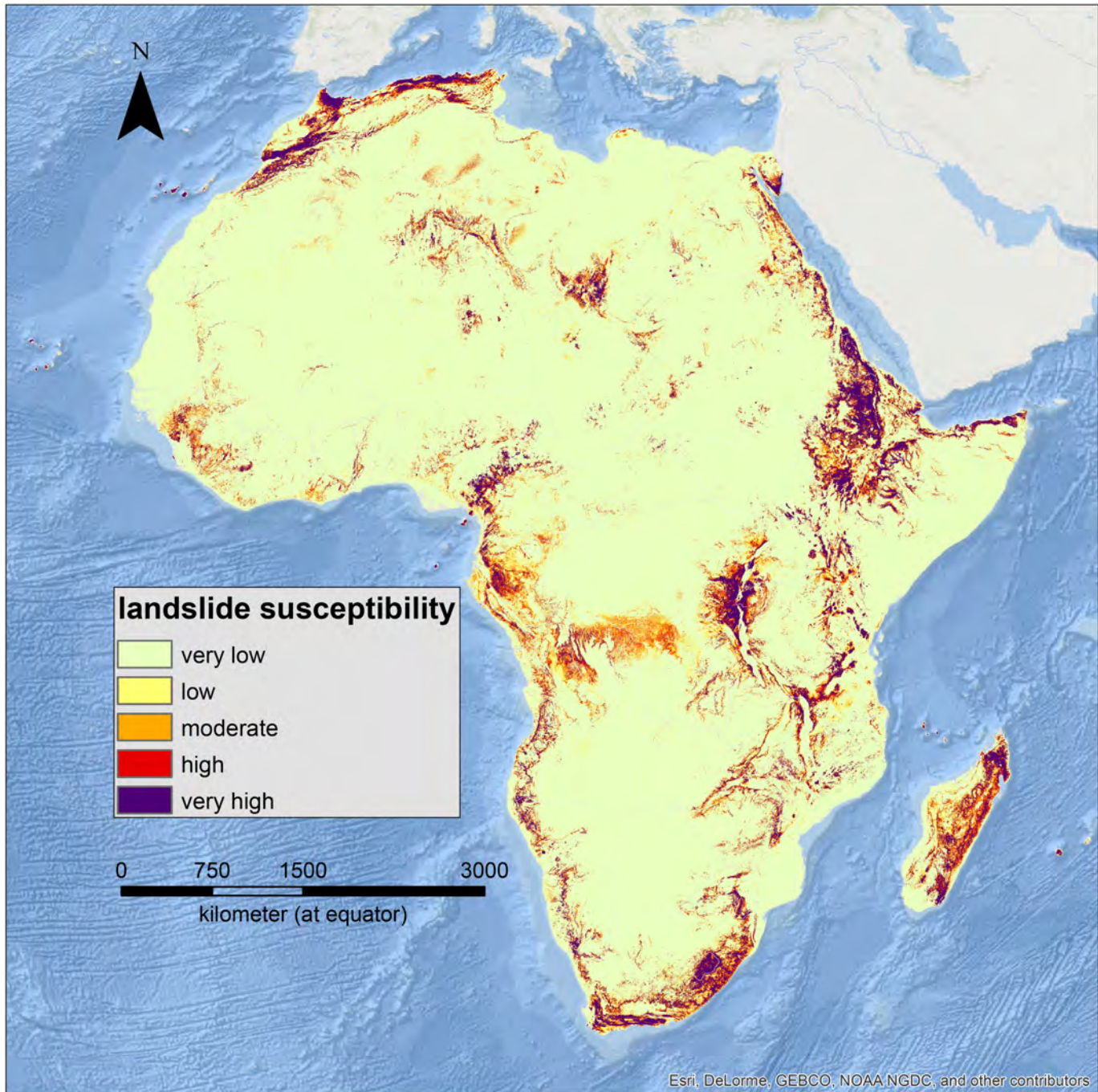


Figure 6

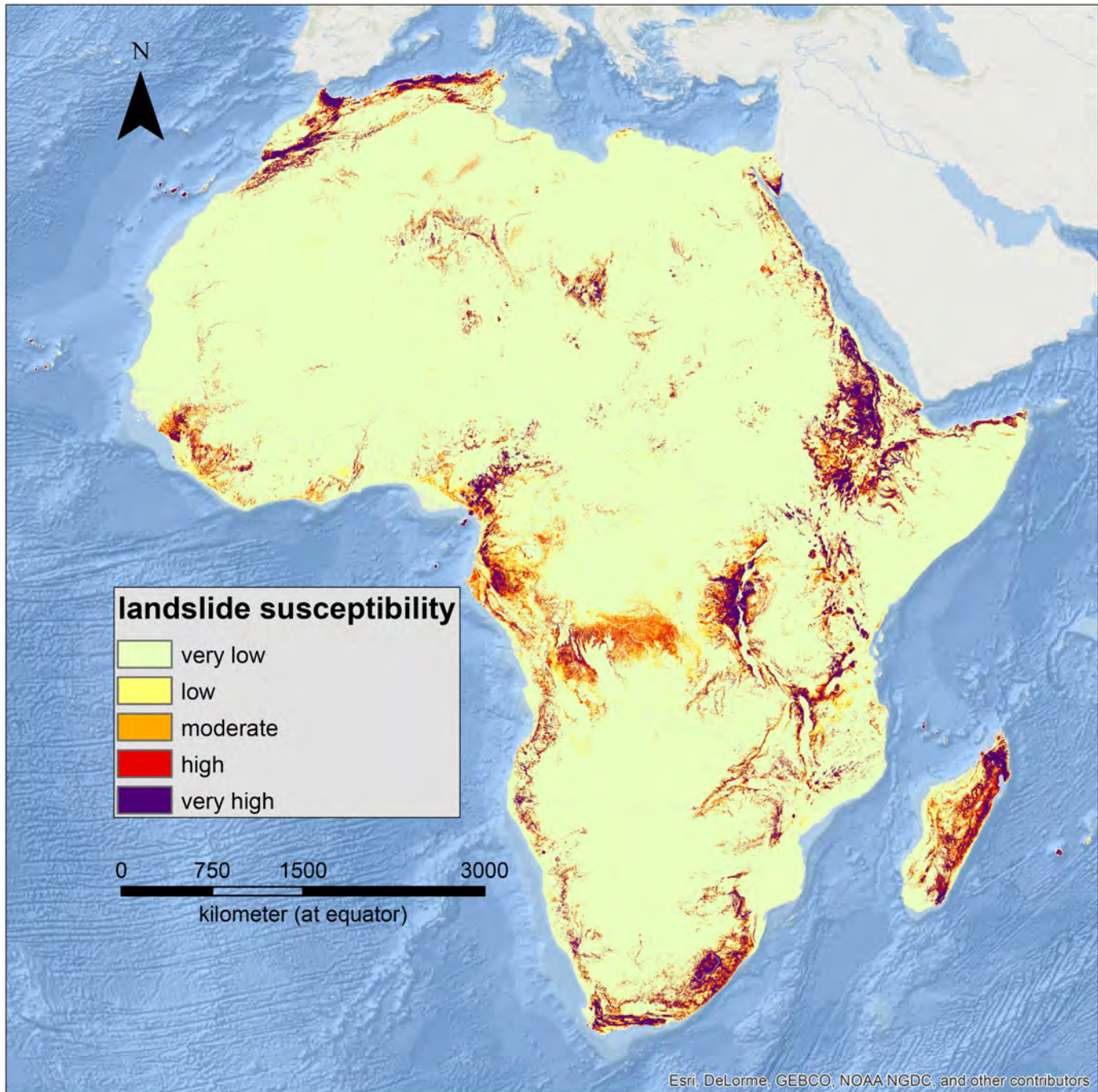


Figure 7

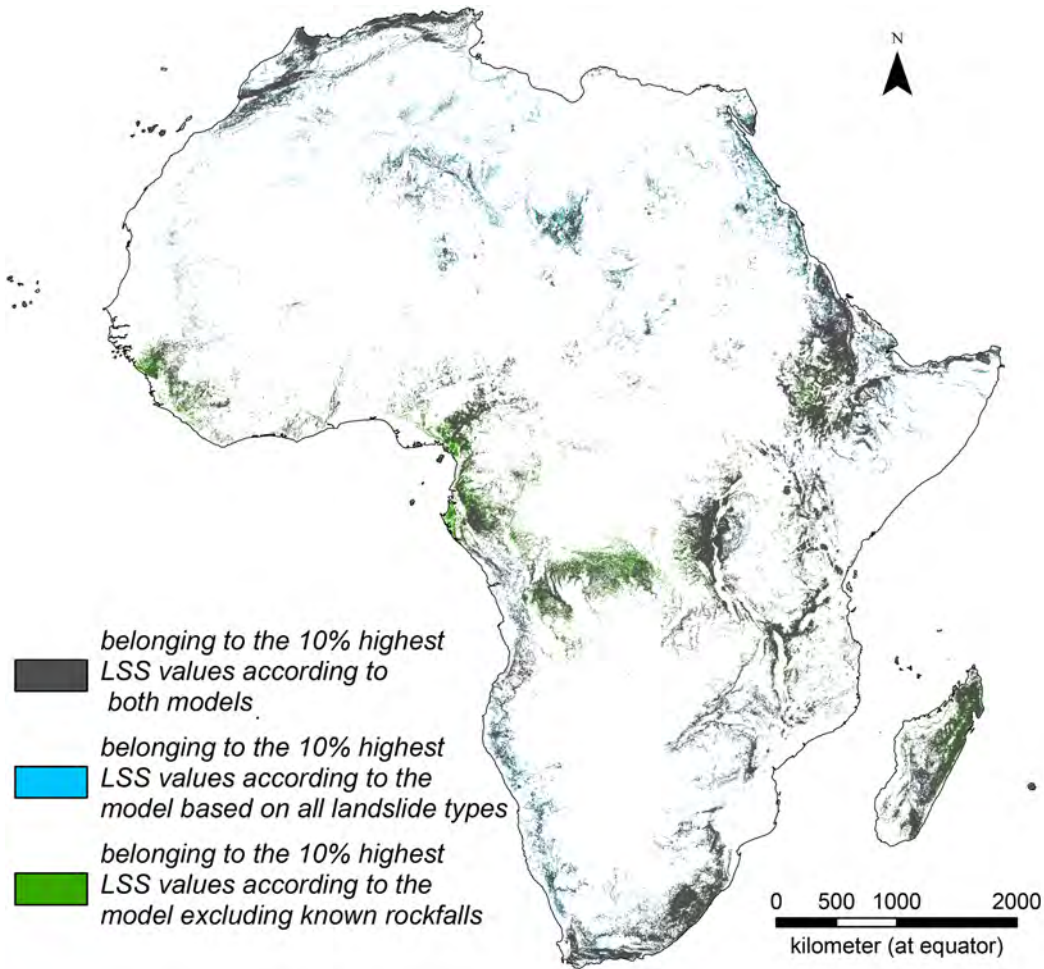


Figure 8

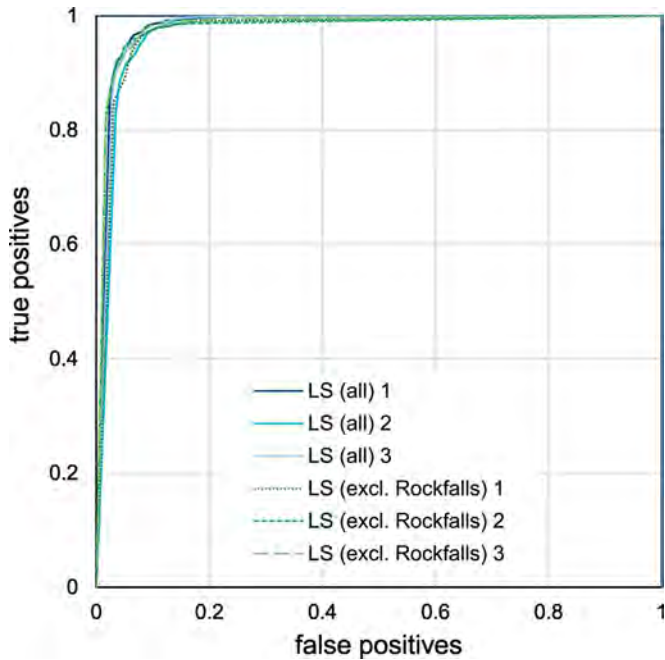


Figure 9

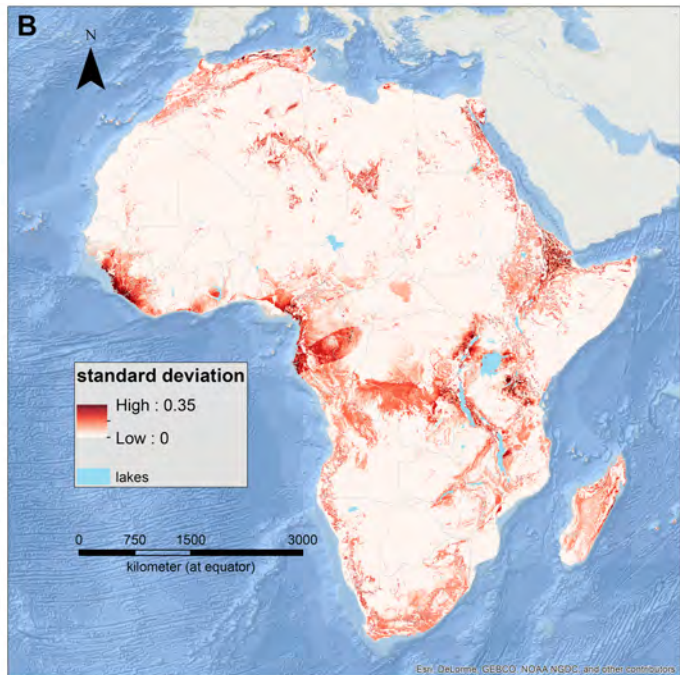
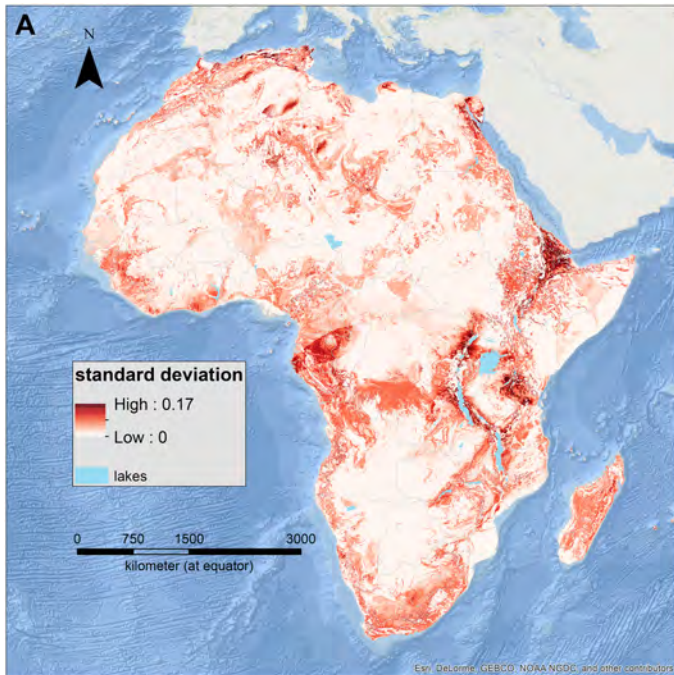


Figure 10

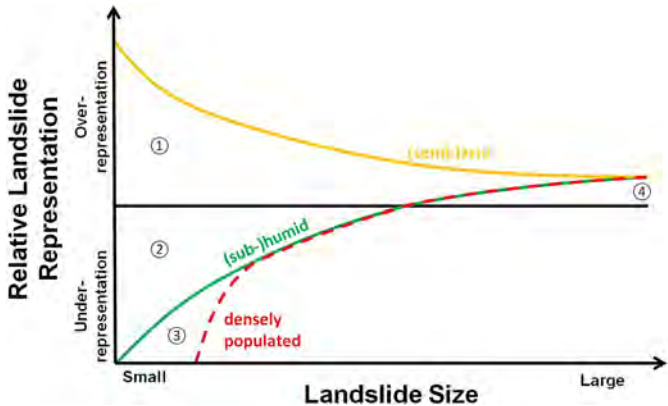


Figure 11

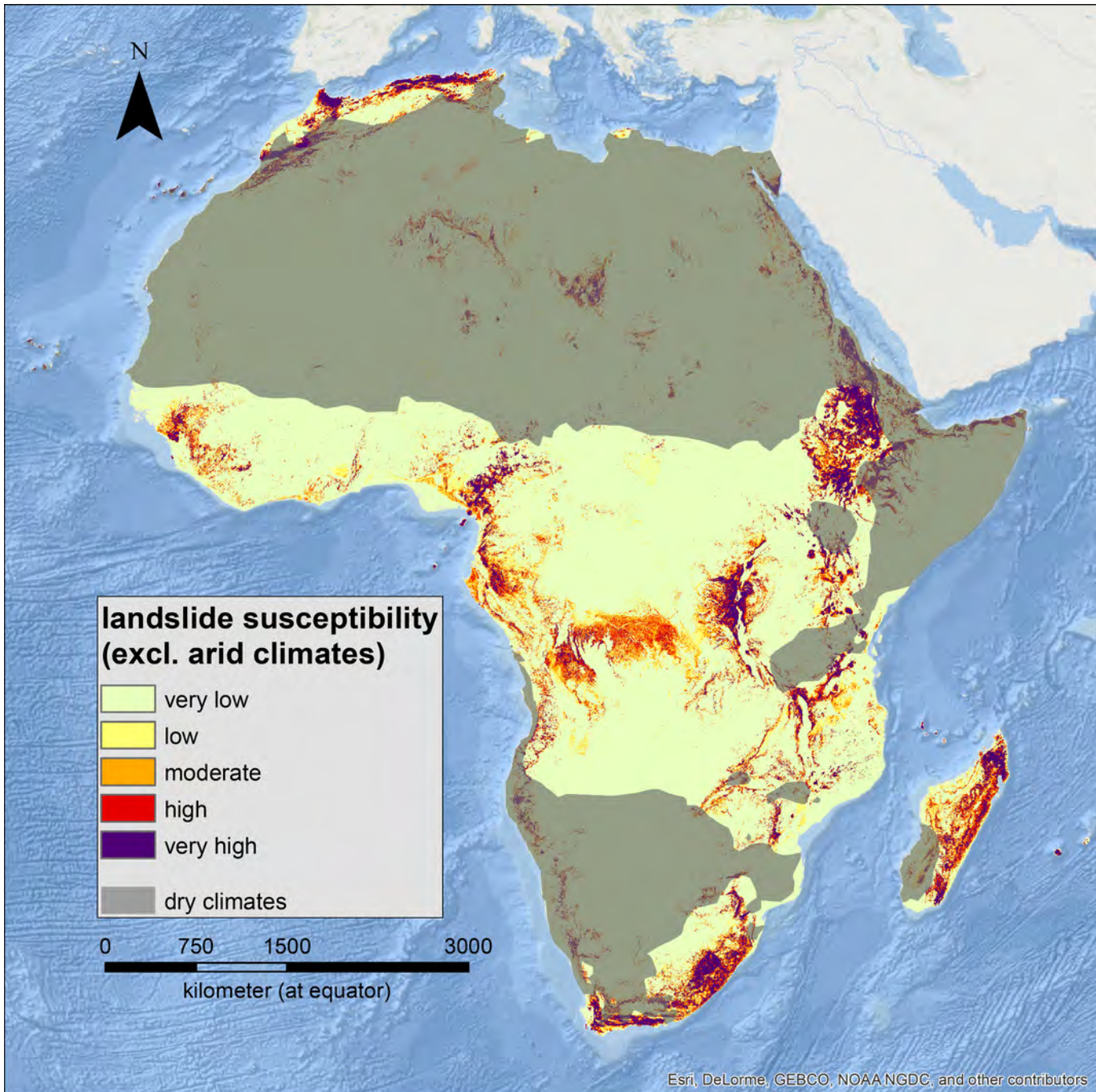


Figure 12

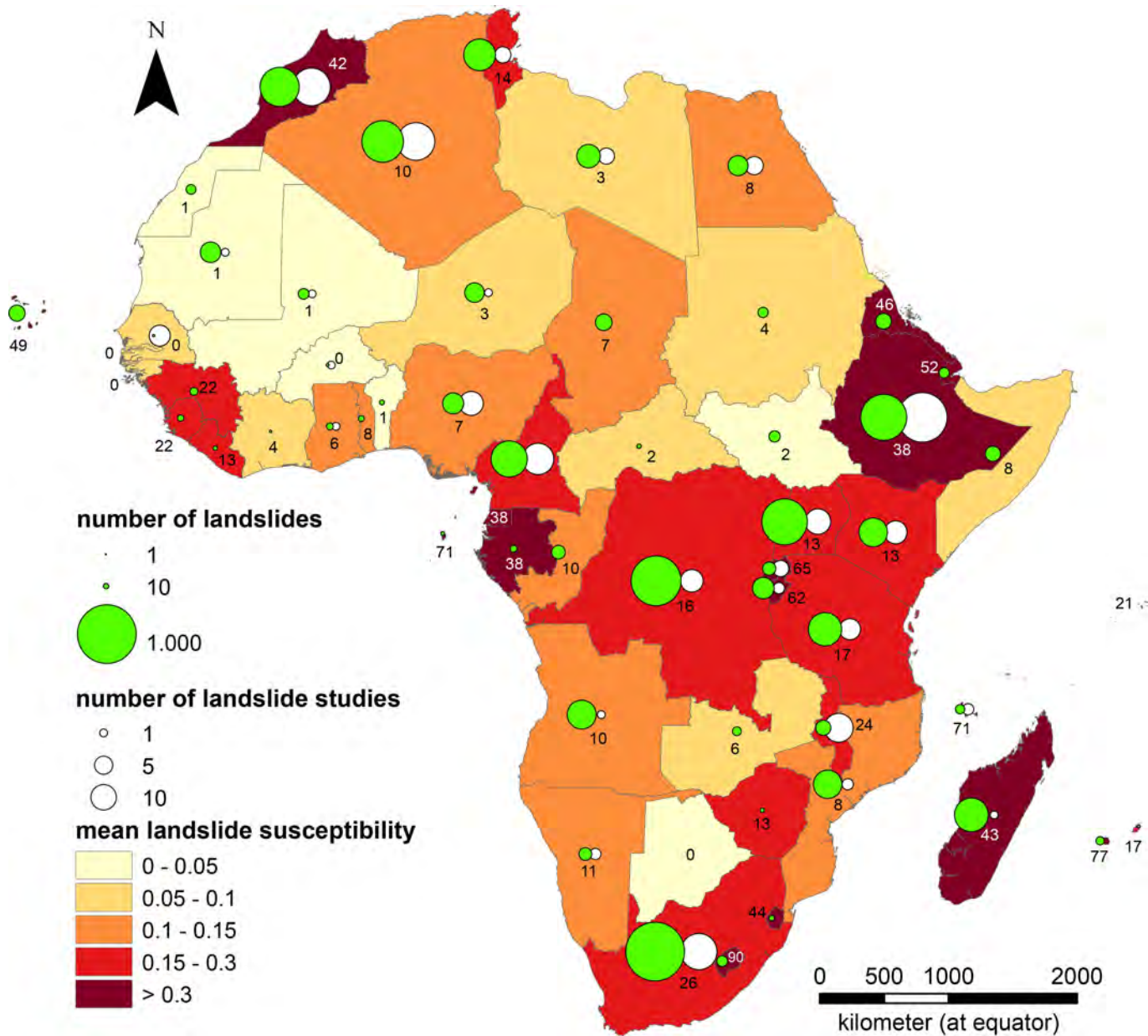


Figure 13

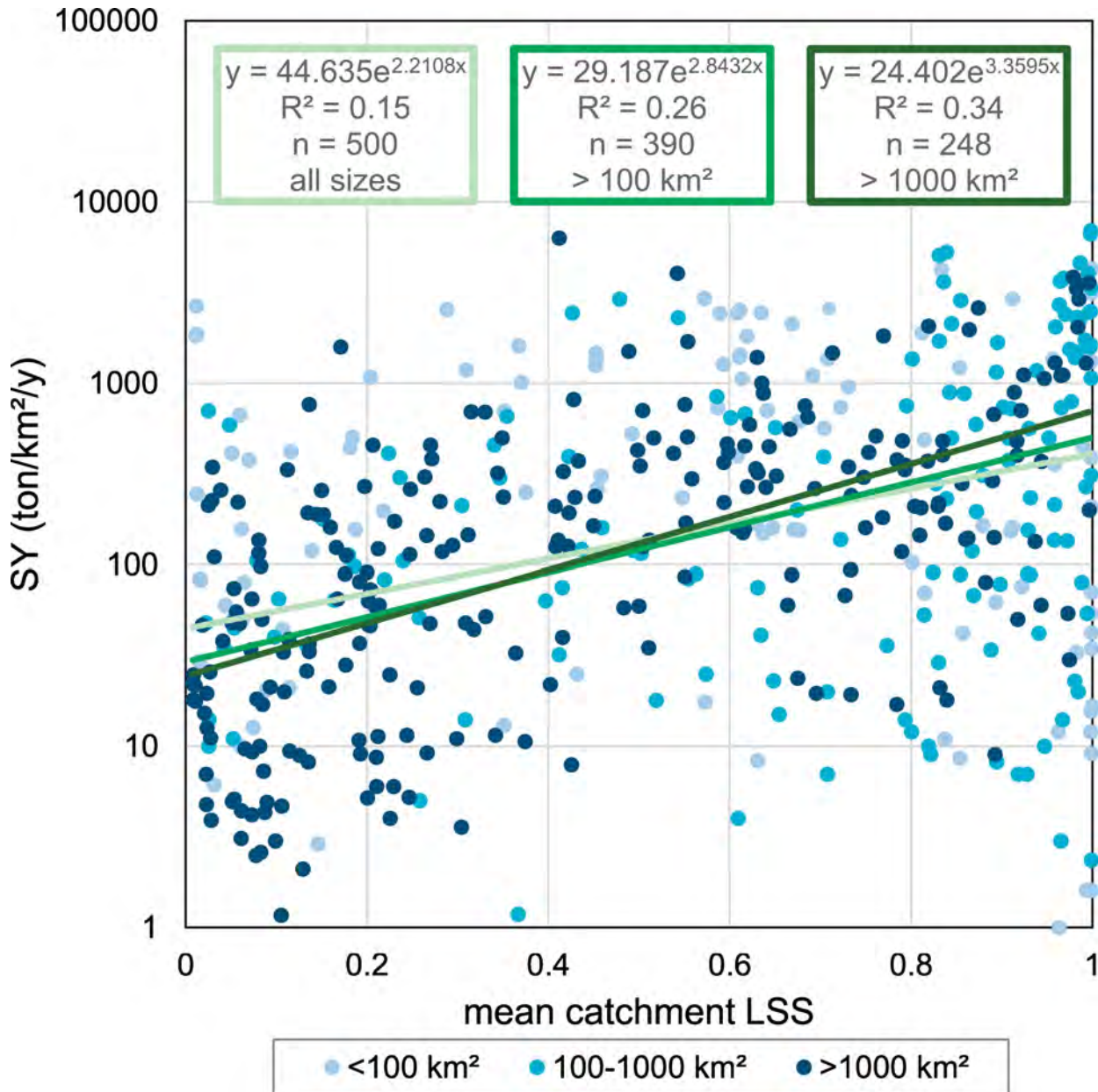


Figure 14

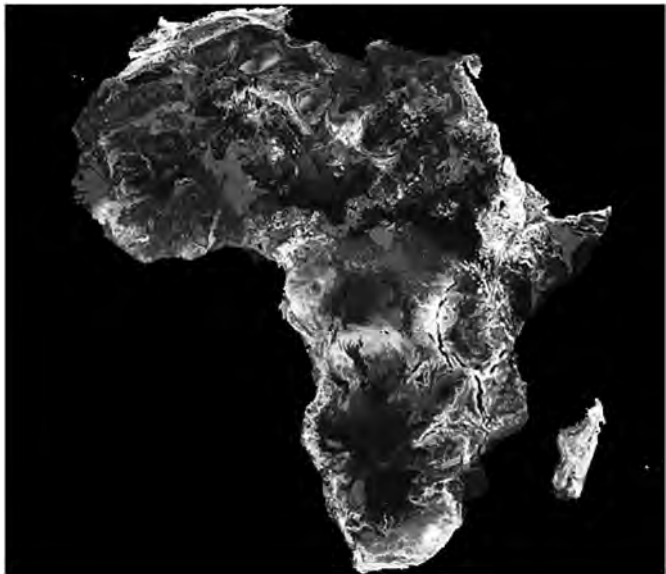


Figure 15

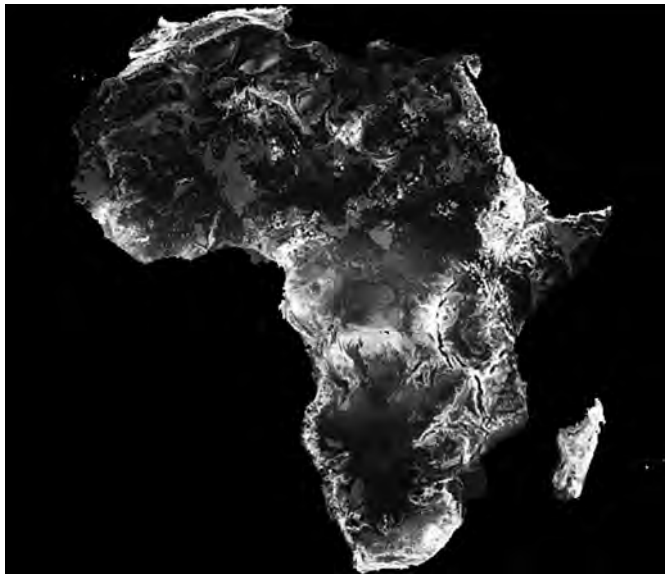


Figure 16